Biaxial Concrete Column Analysis and Nonlinear Stress-Strain Curves

By

John Southard, M.S., P.E.

PDHLibrary Course No 2018031
4 PDH HOURS

TABLE OF CONTENTS

Page

ABSTRACT v

CHAPTER

1 INTRODUCTION 1

2 MATERIAL BEHAVIOR 5

2.1 Concrete 5
2.2 Nonlinear Stress-Strain Relationships for Concrete 5
2.3 Additional Modeling Assumptions 11

3 NUMERICAL COMPUTATION OF INTERACTION DATA 11

3.1 Generation of the Three-Dimensional Failure Surface 11
3.2 Computation of Failure Lines 12
3.2.1 Rotation of the Cross Section 12
3.2.2 Computation of Failure Points on the Failure Line 13
3.3 Constant-Load Biaxial Moment Interaction Diagrams 16
3.4 Applicability of Interaction Diagrams 19

4 NONLINEAR CONCRETE STRESS-STRAIN CURVES 20
4.1 Stress Distributions 20
4.2 The k_3 Factor 20

5 COMPARISONS BETWEEN EXPERIMENTALLY MEASURED AND NUMERICALLY COMPUTED SECTION CAPACITY DATA 25

5.1 Mattock and Kriz 25
5.2 Hognestad 26
5.3 Veist, Elstner, and Hognestad 28
5.4 Lee and Son 28
5.5 Hsu's 1985 Investigation 29
5.5 Hsu's 1992 Investigation 30

6 CONCLUSIONS AND COMMENTARY 40

APPENDIX

A PROGRAMMING FUNCTIONS 43

REFERENCES 46

BIOGRAPHICAL SKETCH 48

Abstract of Thesis Presented to the Graduate School
of the University of Florida in Partial Fulfillment of the
Requirements for the Degree of Master of Engineering

A NUMERICAL PROCEDURE FOR COMPUTING BIAXIAL LOAD-MOMENT INTERACTION DIAGRAMS USING NONLINEAR STRESS-STRAIN RELATIONSHIPS

By

John Harold Southard

May 2003

This thesis presents a numerical procedure for computing a three-dimensional failure surface for reinforced and prestressed concrete sections of arbitrary cross-sectional shape. Two-dimensional interaction diagrams may be extracted from this failure surface to suit the needs of designers and researchers. Construction of the failure surface is accomplished by computing section capacities corresponding to numerous orientations and positions of the neutral axis. For each resulting strain distribution across the section, stresses and forces in the constituent materials are computed in order to determine the section capacity. This is done in part by using piecewise integration of nonlinear concrete stress-strain curves across discretized concrete segments (which, in sum, form the shape of the compressive zone). A comparative study was performed to validate the proposed computational model by comparing program-generated data to experimental data published in the literature. The nonlinear material models used to represent concrete

and steel behavior are presented, along with a discussion of the ramifications of using such relationships for design. During this study, it has been determined that improved design guidelines need to be developed in order to make the use of nonlinear concrete stress-strain

curves a routine procedure in the structural design of beam-columns. To address this need, guidelines are suggested that account for differences between the in situ strength of concrete and that of reference test cylinders.

CHAPTER 1
INTRODUCTION

Interaction diagrams are a powerful numerical tool by which designers can evaluate the load-bearing capacity of beam-columns (Figure 1). Any load point that falls within the region bounded by the three-dimensional failure surface is considered to be an acceptable load condition.

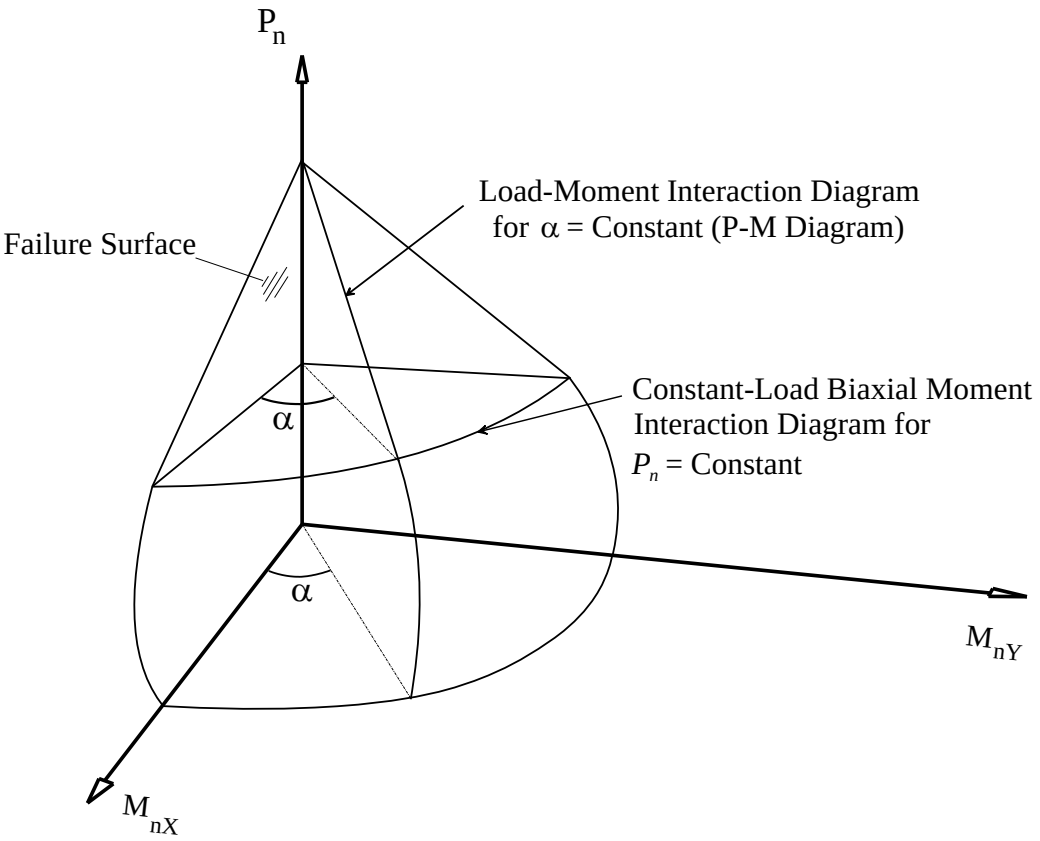

Figure 1. Three dimensional failure surface (interaction diagram)

The region within the failure surface represents a condition in which the effects of an applied structural loading are less than the capacity of the member. Load points

occurring on the failure surface represent a condition where section capacity has been reached and concrete begins to crush. A load point located outside the failure surface represents a load condition causing failure of the member.

For concrete members, the most commonly used two-dimensional interaction diagram is the load-moment (P-M) interaction diagram. This type of diagram is a plot of the axial load capacity (P_n) versus the resultant moment capacity (M_n). The plot creates a boundary referred to as a failure line. All failure lines occur along the three-dimensional failure surface. Another type of interaction diagram often used by designers is the constant-load biaxial moment interaction diagram. This diagram is commonly used for assessing the capacity of beam-columns under biaxial flexure. Constant-load biaxial moment interaction diagrams consist of a plot (failure line) of the moment capacity (M_{nY}) about the section Y-axis versus the moment capacity (M_{nX}) about the section X-axis at a specified axial capacity (P_n).

Procedures have been published in the literature for computing interaction diagrams for columns of arbitrary cross-sectional shape and subjected to biaxial bending and compressive axial loads (e.g. Rodriguez-Gutierrez and Aristizbal-Ochoa 1999). In this thesis, an innovative new numerical method is presented that generates three-dimensional failure surfaces for use in beam-column analysis. Implementation of the proposed method has been accomplished through the development of a multi-module program that was provided by the Florida Department of Transportation and is publicly available for download at their structural engineering software website (Ansley 2001). Many of the modular component functions of the program can be modified or replaced to suit individual needs. The computational algorithm and its programmatic implementation provide engineers with a new and versatile tool for analyzing concrete beam-columns.

For example in concrete research, the stress-strain function used in the proposed model can be modified to improve the predictive capability of the program for unusual or experimental materials. Deriving more exact stress-strain relationships for a specific concrete mix design, as outlined by Wang (1978), will help researchers isolate the effects of variables such as the effects of casting orientation or admixtures. Using the program presented herein, researchers will be able to use stress-strain curves specifically developed for the materials being studied. Design engineers will be able to use irregular cross-sectional shapes and account for section voids in their designs that previously could not be taken into account in a convenient fashion.

The numerical procedure implemented in the program and presented in this thesis generates a three dimensional failure surface. Load-moment interaction diagrams can then be extracted from the three dimensional failure surface by taking a slice of the surface at a constant angle (α) where α is the angle measured from the plane of the section X-axis to the desired plane of the resultant moment capacity (Figure 1). Constant-load biaxial moment interaction diagrams are similarly extracted by taking a slice through the failure surface at a constant axial capacity (P_n). In the past; these diagrams were often generated by computing a limited number of failure points and then using curve-fitting techniques to establish the shape of the diagram. The numerical method presented in this thesis instead generates a complete mesh of failure points using a rational procedure from which two dimensional interaction diagrams can be extracted and is thus not limited by the use of pre-selected curve fitting forms. The effectiveness of the new analysis technique along with the underlying assumptions for material behavior are demonstrated by conducting a comparative study in which analysis results computed by the program are compared to experimental test data obtained from published experimental investigations.

When advances in structural analysis go beyond the scope of current design specifications or normal practice, it is crucial for designers and researchers to understand the assumptions of the analysis procedures and of the design specifications. The comparative study and literature review presented herein will highlight the effects of using nonlinear concrete stress-strain curves in the computation of section capacity in place of the rectangular stress block. Such information will be of value to designers who attempt to use nonlinear analysis procedures for the purpose of evaluating structural strength. The remainder of the thesis discusses issues surrounding the use of nonlinear concrete stress-strain curves in strength calculations so that engineering judgment can be applied in an informed manner.

CHAPTER 2
MATERIAL BEHAVIOR

2.1 Concrete

Most assumptions for material behavior, in the proposed model used to implement the numerical procedure, are conventional. For example, a value of 0.003 is used as the maximum compressive crushing strain of concrete. This value as well as other parameters can be modified to suit the needs of the structural analyst or designer. However, before modifying any of the conventional assumptions in the proposed model, it is imperative that the designer understand the potential ramifications of such changes. Throughout this thesis, concrete stress-strain behavior was modeled with nonlinear stress-strain curves in place of the often-used conventional assumption of an equivalent rectangular stress block.

2.2 Nonlinear Stress-Strain Relationships for Concrete

To demonstrate the effects of nonlinear concrete stress-strain curves on computed capacity and to demonstrate the versatility of the analysis program, three different stress-strain curves are used in this study:

- Hognestad's parabola (Hognestad 1951)
- The stress-strain curve proposed by Collins and Mitchell (1991)
- A modified version of Carreira and Chu's model (Wee, Chin, and Mansur 1996).

Each of these material models is described in detail below. For comparison, all three of the curves are plotted in Figure 2 for selected concrete strengths. Hognestad (1951) used the formula

$$f_c = f'_c \left[2\left(\frac{\varepsilon}{\varepsilon_o}\right) - \left(\frac{\varepsilon}{\varepsilon_o}\right)^2 \right] \quad (1)$$

where

$$\varepsilon_o = 0.002$$

Collins and Mitchell (1991) used the formula

$$f_c = \frac{f'_c \cdot n\left(\frac{\varepsilon}{\varepsilon_o}\right)}{n - 1 + \left(\frac{\varepsilon}{\varepsilon_o}\right)^{n \cdot k}} \quad (2a)$$

where

$$n = \frac{f'_c}{17.2} + 0.8 \quad (2b)$$

$$E_c = 3320\sqrt{f'_c} + 6890 \quad (2c)$$

$$\varepsilon_o = \frac{f'_c}{E_c}\left(\frac{n}{n-1}\right) \quad (2d)$$

$$k = \frac{f'_c}{62} + 0.67 \geq 1.0 \quad \text{when } \varepsilon > \varepsilon_o \quad (2e)$$

otherwise, $k = 1.0$

Wee, Chin and Mansur (1996) used the formula

$$f_c = f'_c \left[\frac{k_1 \beta \left(\frac{\varepsilon}{\varepsilon_o} \right)}{k_1 \beta - 1 + \left(\frac{\varepsilon}{\varepsilon_o} \right)^{k_2 \cdot \beta}} \right] \quad (3a)$$

where

$$E_{it} = 10200 f'^{\frac{1}{3}}_c \quad (3b)$$

$$\varepsilon_o = 0.00078 f'^{0.25}_c \quad (3c)$$

$$\beta = \frac{1}{1 - \left(\frac{f'_c}{\varepsilon_o E_{it}} \right)} \quad (3d)$$

$$k_1 = \left(\frac{50}{f'_c} \right)^{3.0} \leq 1.0 \quad \text{when } \varepsilon > \varepsilon_o \quad (3e)$$

otherwise, $k_1 = 1.0$

$$k_2 = \left(\frac{50}{f'_c} \right)^{1.3} \leq 1.0 \quad \text{when } \varepsilon > \varepsilon_o \quad (3f)$$

otherwise, $k_2 = 1.0$

In the above equations, f'_c is the peak in situ compressive strength (MPa) of the concrete, f_c is the compressive stress at a particular strain level, and ε is the strain. Other factors such as n and various k factors control the shape of the stress-strain curves.

The stress-strain relationships presented in Collins and Mitchell (1991) and Wee, Chin and Mansur (1996) are for use with normal strength and high strength concrete. Research has shown that the Hognestad curve, while popular and easy to use, should only be used for normal

strength concrete (e.g. Wee, Chin, and Mansur 1996). The effects of using nonlinear stress-strain curves on beam-column behavior will be shown later by comparing results computed using the three different stress-strain curves.

2.3 Additional Modeling Assumptions

In addition to the concrete related assumptions discussed above, the implementation of the proposed model in this study was also based upon the following assumptions:

- **Plane sections remain plane during flexure.**
  This is Bernoulli's hypothesis that sections remain plane after loading resulting in a linear strain distribution across the cross-section

- **Bond between steel reinforcement and concrete is perfect.**
  There is no slip at the interface between different materials in the cross-section.

- **Concrete has no tensile resistance.**
  All concrete in the tension zone is assumed to be fully cracked at ultimate strength. Tension stiffening contributions are neglected

- **Shear and torsion deformations are not considered in stress computations.**
  The proposed model only accounts for axial and flexural stresses.

- **Confinement effects developed by steel reinforcement are not considered.**
  Spiral reinforcement can provide confinement of the core of a column which can increase ultimate strength despite spalling of the cover material. This increase in strength is conservatively neglected in the proposed model.

- **The ultimate compressive strain of concrete (ε_{cm}) is assumed to be 0.003.**
  Past research indicates that the maximum compressive strain of concrete varies with respect to loading rate and concrete mix type. For design and analysis purposes, however, research has repeatedly shown 0.003 to be a safe lower bound value (e.g. Lee and Son 2000).

- **Strain hardening effects are not considered.**
  The stress-strain relationship of mild steel reinforcement is elastic, perfectly plastic in both compression and tension.

- **For prestressed tendons, strain is found by the following expression:**

$$\varepsilon_{ps} = \varepsilon_c + \varepsilon_{ep} + \varepsilon_{cp} \tag{4}$$

where, ε_c represents change of strain in the tendons caused by external loads, ε_{ep} is the tendon strain due to initial effective prestress, and ε_{cp} is the change in strain caused by deformation of the section under the effect of prestress force.

- **For prestressing strands, the stress-strain relationship is modeled by the Ramberg-Osgood function (Collins and Mitchell 1991).**

The general form of the stress-strain relationship for prestressing strands is shown below;

$$\sigma_p = E_p \varepsilon \left(A + \frac{1 - A}{\left(1 + \left(B\varepsilon\right)^C\right)^{1/C}} \right) \leq \sigma_{pu} \tag{5}$$

where the parameters E_p, A, B, and C, and σ_{pu} establish the shape of the stress-strain curve. Values used for the low-relaxation and stress-relieved prestressing strand are given in Collins and Mitchell (1991). For A722 steel, the ultimate stress σ_{pu} is 1860MPa (270ksi), E_p = 200,000 MPa (29,000 ksi), A =0.0043, B =192, and C =4.19.

- **The k_3 factor accounts for the effects of casting position**.

The k_3 factor is an in situ adjustment factor for concrete strength. It accounts for compaction and water gain due to casting position. All other variables affecting the in situ strength of concrete are assumed to be unity or are accounted for in the design specifications via resistance factors.

- **The reference centroid is chosen as the plastic centroid.**

The reference centroid is the point in the cross-section about which section moments are computed. Flexural capacities of the section about the x and y axes are computed with respect to the reference centroid. In this study, the reference centroid is chosen to match the location of the plastic centroid.

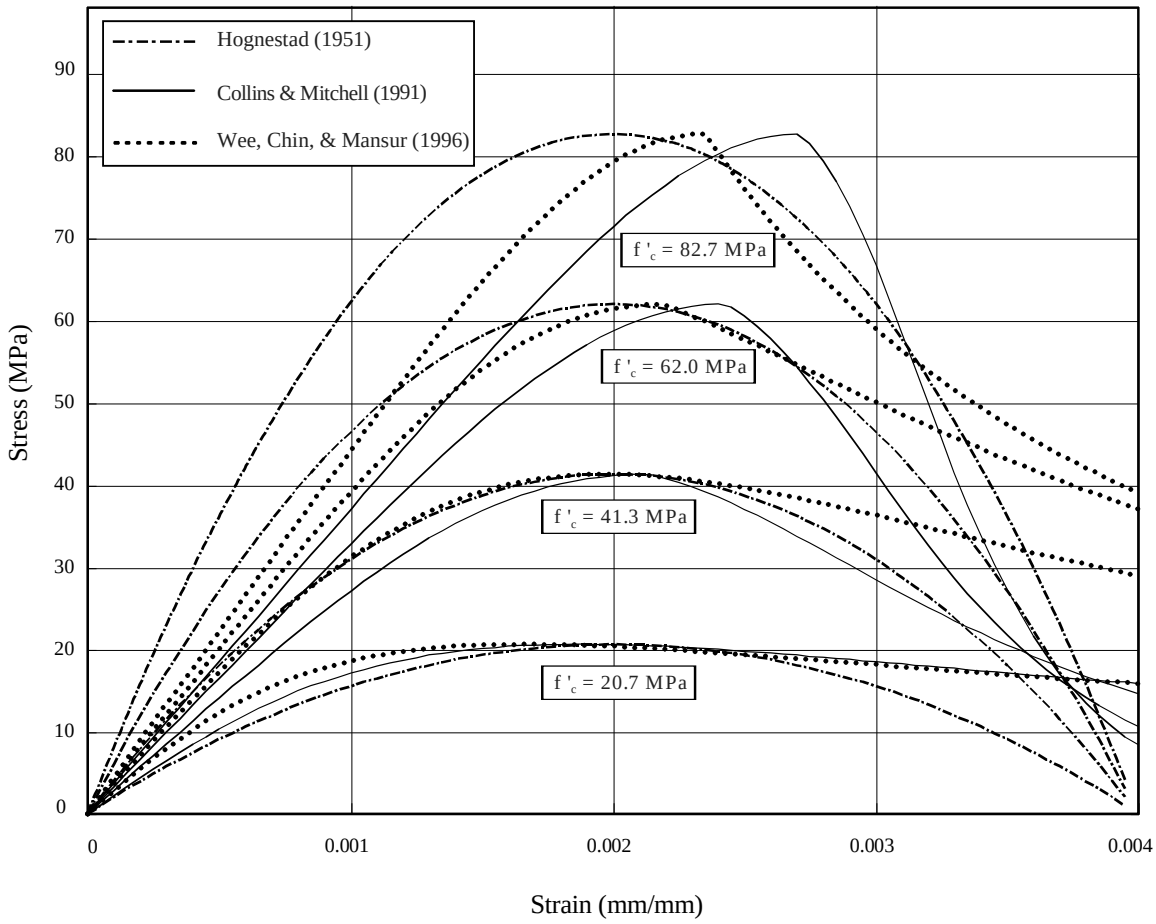

Figure 2. Comparison of nonlinear stress-strain relationships for concrete

CHAPTER 3
NUMERICAL COMPUTATION OF INTERACTION DATA

3.1 Generation of the Three Dimensional Failure Surface

The three dimensional failure surface for a given cross-section is created by combining numerous failure lines corresponding to different angles of rotation (θ) of the neutral axis (See Figure 3). Plotting a series of failure lines yields a mesh of failure points on the failure surface from which two dimensional interaction diagrams can be extracted. The failure lines generated by fixing the neutral axis orientation differ from those found on load-moment interaction diagrams in that the resultant moment capacities do not necessarily lie on a constant plane defined by α (Figure 1).

Each failure line is computed by imposing an angle of rotation θ for the neutral axis and then moving the neutral axis incrementally across the cross-section. For each position, the section capacity is computed and thus a failure point on the failure line and failure surface is found. To calculate the initial point $(P_{n1}, M_{nX1}, M_{nY1})$ on the failure line for each angle θ, the neutral axis is set to a distance far enough from the reference centroid to cause a strain distribution that is essentially uniform across the section. As the neutral axis is moved across the cross-section for a fixed θ, the axial load capacity (P_n) will decrease and the section moment capacities $(M_{nX} \text{ and } M_{nY})$ will increase. For each location of the neutral axis, the axial load capacity and local moments $(M_{nx} \text{ and } M_{ny})$ are computed with respect to the corresponding strain distribution. The local moments are then transformed into global section moments $(M_{nX} \text{ and } M_{nY})$ as will be discussed later. Connecting failure points for each location of the neutral axis yields a failure line on the three dimensional failure surface. After each failure line

is created, the neutral axis is rotated and the above process is repeated until enough failure lines are generated to sufficiently describe the failure surface.

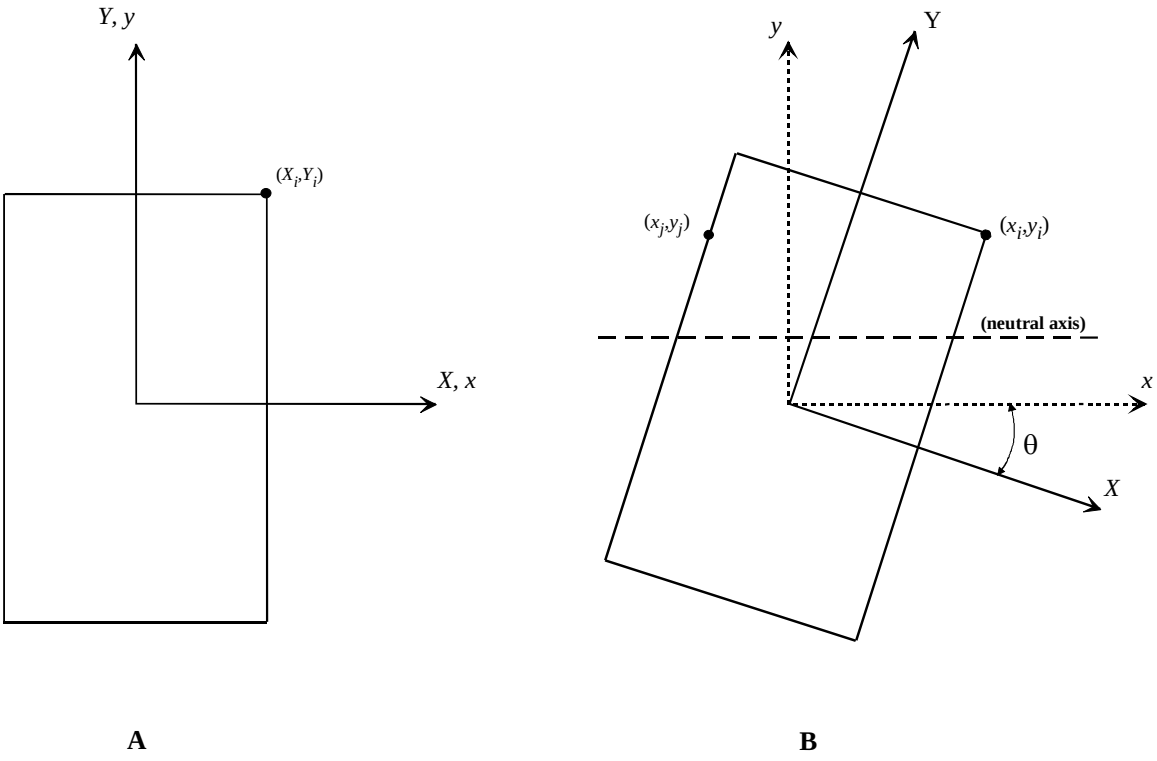

Figure 3. Neutral axis orientation. A) Before rotation. B) After rotation

3.2 Computation of Failure Lines

3.2.1 Rotation of the Cross Section

Before the capacity of the section can be determined, the coordinates describing the cross-section must be rotated and the cross-section discretized. In Figure 3 the global axes are represented by capital letters X and Y, while the local axes are represented by lowercase letters x and y. The orientation of the neutral axis is defined by θ, which relates the rotation of the

section's local axes to its global axes. The numerical procedure always defines the neutral axis as a horizontal line $(y = \text{constant})$ in the local coordinate system and then moves it by vertical increments through the section. To accommodate this process for a given angle θ, the cross-section and the global axes are rotated in the reverse direction about the local axis (Figure 3b). Rotation of all points in the cross-section (X_i, Y_i) is a component of the program. The coordinate positions rotated include those used to define the shape of the section, voids within the section, reinforcement locations, and the reference centroid. The new coordinates are in terms of (x_i,y_i) with respect to the local axis as seen in Figure 3b.

Coordinates defining the shape and voids are arranged in a closed contour format. In other words, the first and last coordinate of each contour defining a shape or void must be the same. After rotation, each coordinate on a contour will have a mirrored coordinate position at the same height or local *y* value created. Thus for each global point (X_i,Y_i) on a contour, a rotated local contour point (x_i,y_i) is created along with another point (x_j,y_j) where y_j equals y_i. The matrices which contain these new coordinates are then rearranged appropriately to prepare them for discretization. Once prepared, trapezoid shaped segments are created by making horizontal slices through the cross section connecting (x_i,y_i) to (x_j,y_j) coordinates.

3.2.2 Computation of Failure Points on the Failure Line

Once the section has been discretized for a given neutral axis orientation, the maximum and minimum local y coordinates for the cross-section are found. The starting and ending positions of the neutral axis are than determined from the difference between these two values. The neutral axis is incrementally moved through the section in the local *y*-direction and for each

position the section capacity or failure point (P_n, M_{nx}, M_{nY}) is found. A failure line emerges when each of the failure points is connected by a linear line (Figure 4).

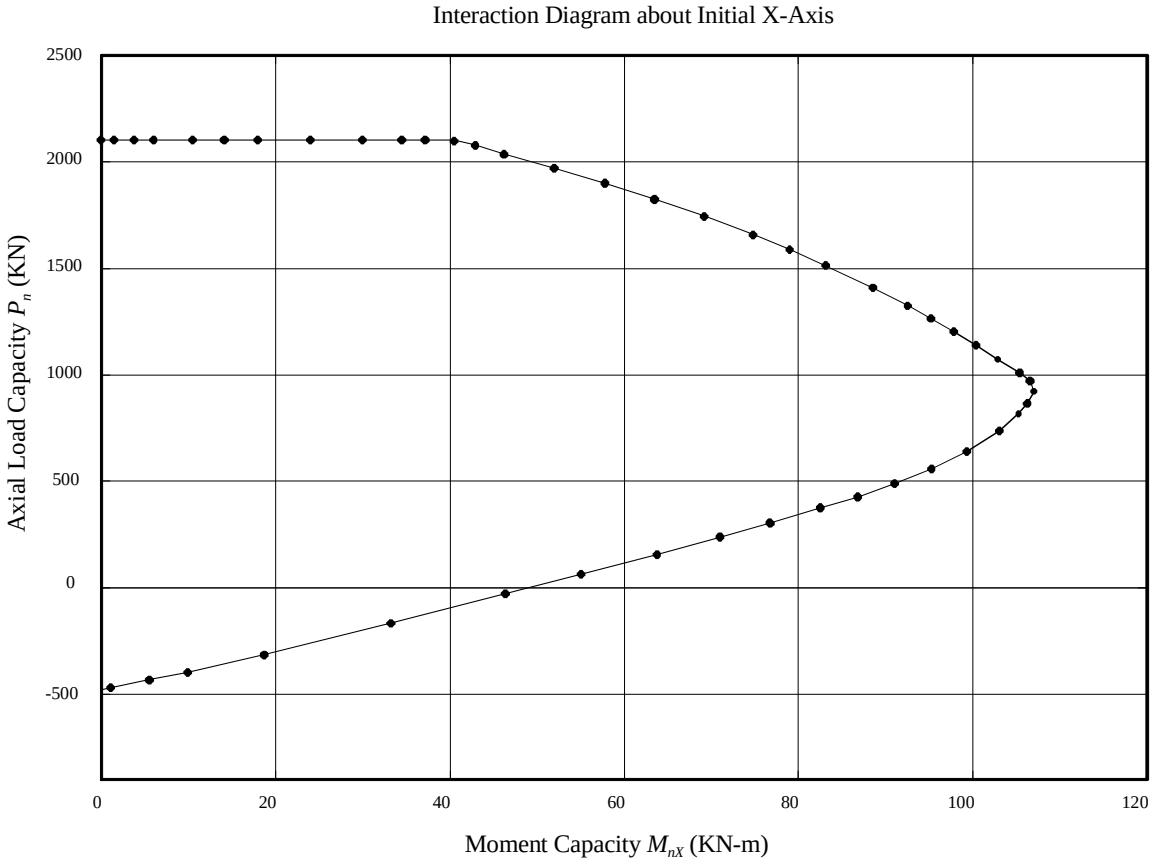

Figure 4. Construction of a failure line

To calculate each failure point for a neutral axis position, the strain distribution across the cross section is determined and the forces in the underlying materials (e.g. mild steel, prestress, and concrete segments) making up the cross-section are determined. The sum of these forces equals the axial load capacity (P_n) . Summing the moments created by these forces in both directions about the reference centroid (plastic centroid) yields the local moments $(M_{nx} \text{ and } M_{ny})$ (Eqs. (7) and (8)).

$$P_n = P_{(concrete)} + P_{(mild\ steel)} + P_{(prestress)} \quad (6)$$

$$M_{nx} = M_{x(concrete)} + M_{x(mild\ steel)} + M_{x(prestress)} \quad (7)$$

$$M_{ny} = M_{y(concrete)} + M_{y(mild\ steel)} + M_{y(prestress)} \quad (8)$$

Using the angle θ, the local moments are then transformed into the global section moments $(M_{nX}\ and\ M_{nY})$. The values computed from Eqs. (6), (9) and (10) represent one failure point on the failure line (P_n, M_{nx}, M_{nY}).

$$M_{nX} = M_x \times \cos(-\theta) + M_y \times \sin(-\theta) \quad (9)$$

$$M_{nY} = -M_x \times \sin(-\theta) + M_y \times \cos(-\theta) \quad (10)$$

The equations above are a function of the forces developed in the constituent materials. $P_{(mild\ steel)}$ and $P_{(prestress)}$ are calculated by multiplying the stress developed in each bar by the area of that bar. The stress in each bar is computed for the strain level at the center of each bar. Concrete forces in the concrete compression zone (above the neutral axis) are determined by finding the strain at the top, middle, and bottom of each trapezoidal shaped segment created during discretization. With the strain at each location known, the compressive stress acting on each segment can be determined using the stress-strain curve of the in situ concrete. Using the nonlinear concrete stress-strain function and numeric integration techniques (Simpson's rule), the stresses are multiplied and summed accordingly to compute the compressive force acting on each trapezoidal segment. The compressive forces developed in each segment are then summed

to determine $P_{(concrete)}$. Next, $M_{x(concrete)}$ and $M_{y(concrete)}$ are computed as the sum of the moments from each segment taken about the reference centroid.

3.3 Constant-Load Biaxial Moment Interaction Diagrams

By performing the steps described above, the three dimensional interaction diagram is created. At a constant axial load capacity P_n , the known points (M_{nX}, M_{nY}) on each failure line are connected by linear lines to construct a constant-load biaxial moment interaction diagram (Figure 5). The failure line for a constant-load biaxial moment interaction diagram will be referred to herein as a load-contour. As the number of neutral axis orientations used to create the failure surface is increased, the resulting load-contours will more closely resemble the true curvilinear nature of the section's three-dimensional failure surface (Figure 5).

Using multiple failure lines to construct constant-load biaxial moment interaction diagrams has distinct advantages. Load-contours constructed from a series of failure lines alleviate the need to utilize curve fitting solutions such as the method of least squares. This in turn allows the proposed model to handle odd section shapes with regard to creating load-contours. Programs utilizing curve-fitting techniques are generally limited to symmetric rectangular or circular shapes. Figure 6 demonstrates the limitation of using curve fitting techniques to generate load-contours versus extracting them from a complete mesh of failure points. The load contour in Figure 6 is for an L-shaped column and was generated by using one hundred different angles of orientation for the neutral axis. The curve fit lines were made to fit failure points based on the neutral axis being rotated in 15 degree increments (twenty-four neutral axis orientations).

The curve fit lines shown in Figure 6 were derived from the following function which was applied separately to each quadrant:

$$\left(\frac{M_{nY}}{M_{oY}}\right)^{\alpha}+\left(\frac{M_{nX}}{M_{oX}}\right)^{\beta}=1.0 \qquad (11)$$

M_{oX} and M_{oY} are nominal moment strengths at the X and Y-axis intercepts of the load contour. α and β are constants that control the shape of the curve fit line, and are found using the method of least squares given a set of known failure points.

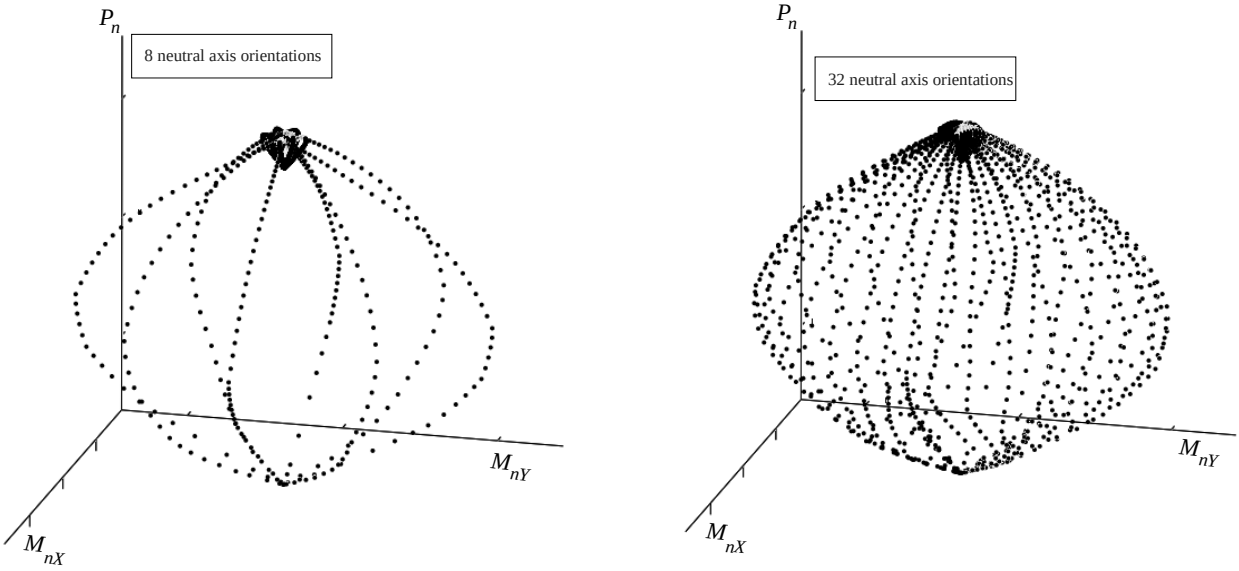

Mesh of Failure Points for Three-Dimensional Interaction Diagrams

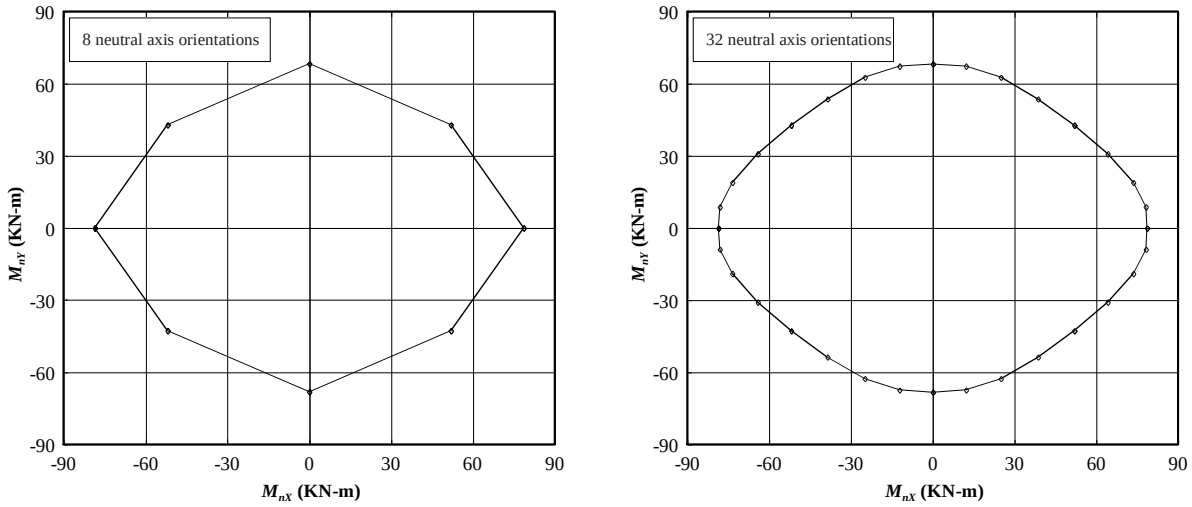

Constant-Load Biaxial Moment Interaction Diagrams (P_n = 1100 KN)

Figure 5. The effect of the number of neutral axis orientations

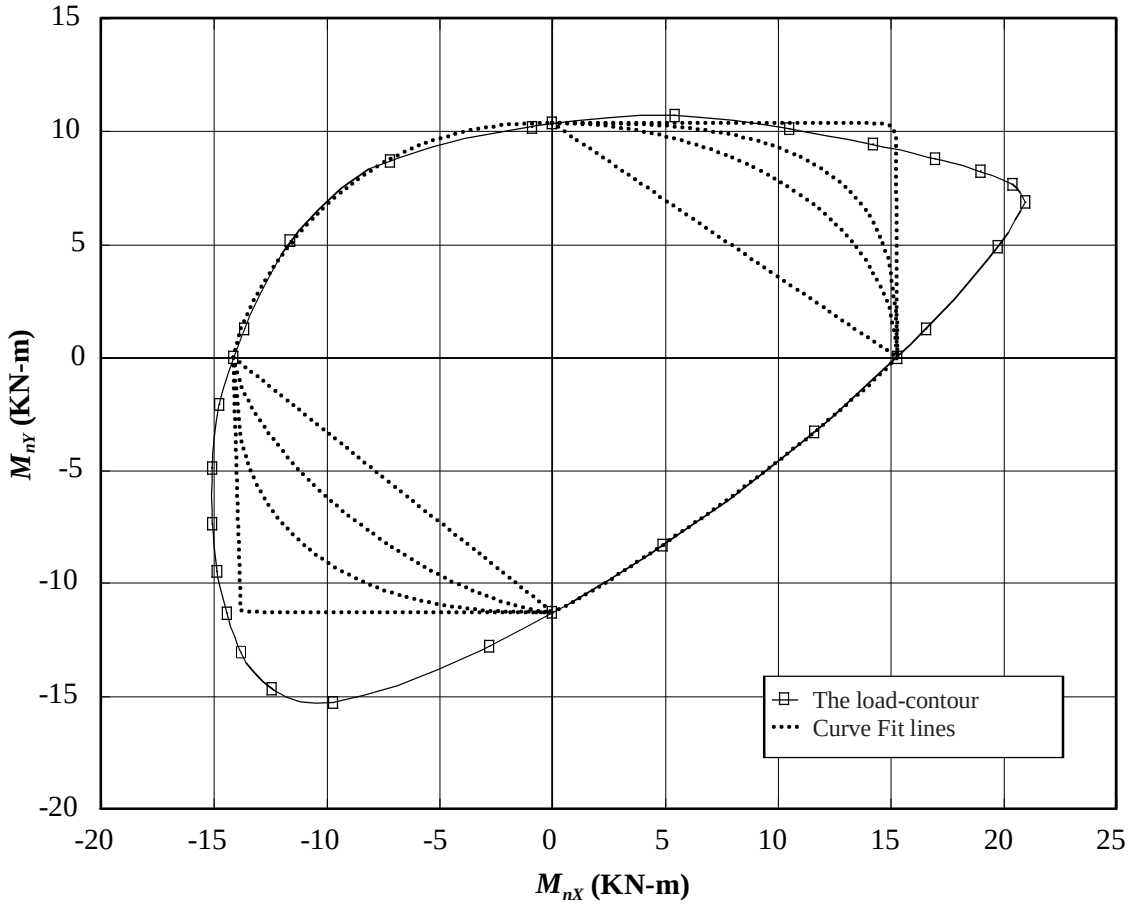

Figure 6. Limitations of curve fit load-contours

In two of the quadrants, the function was unable to duplicate the true interaction diagram. In order for the function to fit irregular shaped load contours, the minimum and maximum coordinates must be known, which are found only by rotating the neutral axis in smaller increments. To generate accurate load-contours from a limited amount of known failure points, the function used to attempt a curve fit must be capable of duplicating the load-contour shape. Creating curve fitting functions for each section shape possible is impractical; therefore the method utilized by the numerical procedure is both more versatile and more accurate.

3.4 Applicability of Interaction Diagrams

The section capacity is computed by summing forces in the materials about the reference centroid. Thus, the reference centroid is the point on the cross section where the resisting axial capacity (P_n) acts. Load points being assessed using the resulting interaction diagrams should have an axial load that is applied at the reference centroid. If this is not the case, an additional coupling moment will be induced as a result of the applied axial load being eccentric to the axial capacity (P_n) resisting the load. Frame analysis programs usually use the elastic centroid as the location of the computed axial loads, thus designers should try to use a reinforcement pattern such that the reference centroid and the elastic centroid coincide. If they do not the designer can either change the location of the reference centroid or carefully adjust column connections with an offset to simulate the induced moment.

CHAPTER 4
NONLINEAR CONCRETE STRESS-STRAIN CURVES

4.1 Stress Distributions

In classic concrete analysis, designers have long used the rectangular stress block. The rectangular stress block parameters α and β are empirical in nature and are based on a lower bound calibration to experimental data from concrete beam tests (Attard and Stewart 1998). The non-linear stress-strain curves used in this study were determined by other researchers by curve fitting through clouds of experimental data. Hence, they are not lower bound and on average should result in a slightly higher capacity versus the ACI rectangular stress block. For pure flexural behavior (beams) this difference is negligible since the stress block has little effect on the resulting moment capacity.

4.2 The k_3 Factor

An additional factor applied to nonlinear concrete stress-strain curves is the k_3 factor. The k_3 factor represents the ratio of the in situ peak compressive stress to the peak compressive stress of the corresponding test cylinder:

$$f'_c = k_3 \cdot f_{cyl.} \tag{12}$$

Proposed values of k_3 vary considerably. Various research has shown that its value ranges from 0.66 to 1.0 (Ibrahim and MacGregor 1997). Many different variables affect the factor, including even its definition. For the purpose of this thesis, k_3 will refer strictly to an adjustment made to account for the effects of casting position. Other variables affecting the in situ concrete strength (and often included in k_3) are heat of hydration, size effects, temperature gradients, formwork type, loading history, and loading rate (Attard and Stewart 1998). The total effect of these other variables is, on average, near unity.

Bartlett and MacGregor (1996) published a paper that showed the values of k_3 to range from 0.95 to 1.03 for various structural elements, such as columns and beams. They determined the maximum compressive strength (f'_c) by using concrete cores obtained from existing structures. Measured core strengths were adjusted to account for statistical differences between core strengths and cylinder strengths. Most cores were taken from the middle of columns. For short columns, cores were taken from the top and bottom, and results for the pairs were averaged. Thus, compaction and the increase in the water flowing to the top of members due to casting position do not appear to have been accounted for in the research. While casting position was not considered, its effects were noted. In the same 1996 publication, Bartlett and MacGregor noted that the measured strength of cores taken from shallow elements (less than 450 mm thick) may have been reduced because of relatively weak concrete near the top of the elements where the cores were taken. The other variables listed above, and often accounted for in the k_3, factor appear on average to be near unity based on their research.

In 1956, Elstner and Hognestad published research on sustained load strength of eccentrically loaded columns. While applying the general stress block theory, it was noted that the k_3 factor was 1.0 when the columns were cast horizontally. A value of 0.85 however, was found to be appropriate when columns were cast vertically (Viest et al., 1956 and Hognestad et al., 1955). Hognestad stated,

> "The principal difference was in the distribution of deflections and in the location of the failure zone. The 1951 columns deflected more above than below mid-height, and failure consistently took place in the upper half, as contrasted by the symmetrical deflection pattern and random location of the zone of failure in the present investigation. The difference is caused by the casting procedures used.

> The 1951 columns were cast in a vertical position; the columns of this investigation, in a horizontal position. Columns cast vertically are weaker near the top as a result of water gain; whereas columns cast horizontally are equally strong along their full height (Viest et al. 1956). ”

The difference in strength, Hognestad explained, could also be attributed to better compaction of concrete near the bottom of columns. Furthermore in Hognestad's 1951 paper, strains measured near the top were greater than those in the bottom implying weaker concrete near the top. These observations were also reported by Slater and Lyse (1931) and Kennedy (1951).

From a literature review, two equations for k_3 were ascertained. Equation 13 was published in 1955 by Hognestad, Hanson and McHenry, while Eq 14 was published by Attard and Stewart in 1998.

$$k_3 = \frac{3900 + 50.8 f'_{cyl.}}{3000 + 119 f'_{cyl.} - 0.81 \left(f'_{cyl.} \right)^2} \tag{13}$$

$$k_3 = 1.05 - 0.0009 f'_{cyl.} \tag{14}$$

Here, $f'_{cyl.}$ is the peak compressive strength of the test cylinders (MPa). The plots of these equations are shown in Figure 7. Equation 13 was intended for use with normal weight concrete, and was curve fitted from experimental results of horizontally cast specimens. Equation 14 was derived for high strength concrete, using experimental results from specimens cast vertically. Thus, direct comparisons of the two equations can not be made. Qualitatively, both curves show k_3 decreasing with strength through most of their applicable concrete strength range.

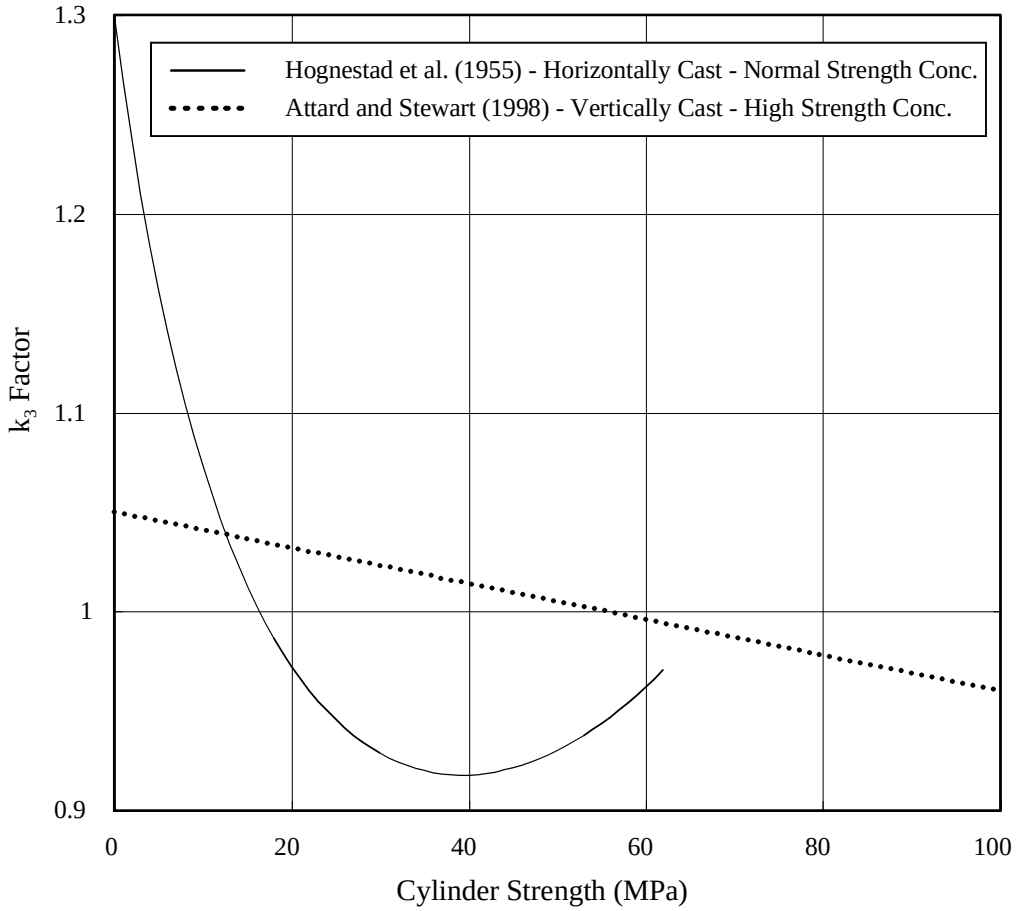

Figure 7. Plots of equations for k_3

From Eq. 13, it can be observed that the k_3 factor for normal weight concrete when cast in a horizontal position ranges from 0.93 to unity. A similar observation was also made by Mansur, Chin, and Wee (1997) for high strength horizontally cast concrete beams. They observed that k_3 was equal to unity on average. Including the research by Bartlett and MacGregor, it seems fair to conclude that for shallow specimens cast horizontally the resulting k_3 value will be close to unity, regardless of concrete strength.

For vertically cast columns and deep beams it seems reasonable to expect k_3 to be significantly less than 1.0. In contrast, Attard and Stewart's 1998 equation agrees closely with

Bartlett & MacGregor's research showing k_3 to be near unity in spite of casting position. The data supporting Eq. 14 was limited to eccentrically loaded high strength columns cast vertically and neglected research data from several other experimental programs. For example, Hognestad's extensive 1951 investigation, highlighted later in this thesis, was not included in the data used to generate Eq. 14. The k_3 values for data from concentrically loaded columns were also much lower and also neglected from the data used to generate Eq. 14 (e.g. Attard and Stewart 1998). Experimental results from eccentrically loaded columns are more reliable however, than those from concentrically loaded columns. Accidental eccentricities occurring with concentrically loaded columns will always yield lower column strength, while for eccentrically loaded columns, the effects of accidental eccentricities average out (Hognestad 1951).

CHAPTER 5
COMPARISONS BETWEEN EXPERIMENTALLY MEASURED AND MUMERICALLY COMPUTED SECTION CAPACITY DATA

To demonstrate the use the proposed model (numerical procedure, programming, and modeling assumptions), data from six experimental programs published in the reference literature were compared to analysis results generated by the program. Program input parameters such as concrete strength, specimen size, specimen shape, and steel reinforcement properties were obtained from the literature for each of the experimental programs. The concrete stress-strain functions used in this study are shown in Appendix A. The results of the comparison study are discussed in the following sections.

5.1 Mattock and Kriz

The original intent of the experimental program conducted by Mattock and Kriz (1961) was to validate the applicability of the rectangular stress block to non-rectangular beams subjected to pure bending. Mattock and Kriz cast six beams with triangular compressive zones (Figure 8) and high steel reinforcement ratios. Concrete strengths ranged from 11.7 to 48.2 MPa. The typical mode of failure, due to the reinforcement ratios used, was crushing of the concrete in the compressive zones. Since these beams were cast horizontally a value of k_3=1.0 was used in the numeric computation process. On average, the predicted moment results of the proposed model compared well with the experimental data. As shown in Table 1, Collins & Mitchell and Wee, Chin, and Mansur's stress-strain models yielded moment capacity comparison ratios of 0.97 and 1.0 respectively. For the rectangular stress block, the comparison ratio was 0.91. The results show that using nonlinear concrete stress-strain curves within the framework of the proposed model yields more accurate moment capacities versus the rectangular stress block when applied to beams with non-rectangular compressive zones. Due to the lower-bound

calibration used to develop the rectangular stress block concept, the capacities thus predicted by it were more conservative than the moment capacities computed with nonlinear stress-strain functions.

5.2 Hognestad

Hognestad's 1951 program was an extensive investigation of 120 eccentrically loaded columns set with pinned ends. These columns were divided into four groups. Columns with concentric loads were excluded because they were loaded through knife edges which results in loads generally 15% lower than when loaded with flat ends (Hognestad 1951). Only the eccentrically loaded columns from Group II are presented in this thesis. Each column was 254 mm^2 (Figure 9) and made of low strength concrete with an approximate slump of 152.4 mm. Group II had a symmetric reinforcement pattern and was reinforced in such a manner that the steel yielded but did not enter the strain hardening region before section failure.

The columns were cast vertically and hence a k_3 value of 0.85 (as suggested by Hognestad) was selected for analysis using the procedure discussed herein. At the time of the Hognestad's original investigation, the descending portion of the stress-strain curve was not known, therefore its shape was approximated so that the analysis results reported in 1951 compared reasonably well with the experimental data. Since experimentally derived nonlinear stress-strain curves are used to generate the analysis data in this thesis, the comparison to test results and the effects of k_3 will be more accurately represented in this study. The applied moment at column failure was computed using the following equation:

$$M = P(e + y_e) \tag{15}$$

where M is the applied moment at column failure, P is the applied axial load at failure, e is the initial eccentricity of the load, and y_e is the measured deflection at mid-height of the column at failure.

As can be seen in Table 2, the moments predicted by the proposed model compared very well with the experimental test data measure by Hognestad. Four different sets of load eccentricities represented four different failure points on the typical load-moment interaction diagram. Higher eccentricities result in lower axial load capacities due to increased flexural compressive stresses. From the data presented in Table 2, several observations can be made:

- Differences in the moment comparison ratios for different stress-strain curves were greater when applied loads had small eccentricities. Columns with low eccentricities behave more like columns than beams and the accuracy of the area under the stress-strain curve or the applied stress block is very important. Thus, the accuracy of the chosen concrete stress-strain curve and the k_3 value become more important as the axial load applied to the column increases (Figure 10).
- A k_3 factor of 0.85 resulted in mean moment capacity ratios of 1.01 and 0.99. Also for each eccentricity group the predicted analysis results compared well to the experimental data.
- The effect of the k_3 value on moment capacities for columns with high eccentricities (nearing pure bending) was negligible, and thus the k_3 factor is insignificant.
- When a k_3 value of 1.0 was used for columns with low eccentricities, moments were over predicted by up to 14%. Thus for columns in pure compression (or high axial loads) using an appropriate k_3 factor is critical.
- Concrete strength did not seem to impact the k_3 values considered in this study.

Figure 10 demonstrates the sensitivity of failure lines to the k_3 factor and the shape of the stress-strain curve. Failure lines for all three stress-strain relationships are shown in Figure 10 and were computed with a k_3 value of 0.85. A failure line using Collins and Mitchell's stress

strain curve and a k_3 value of 1.0 was also plotted to show the impact of changing the k_3 value. When flexural stresses control the load capacity of a section the resulting axial load capacities are low. In this range the shape of the stress block and the k_3 factor have little influence on the shape of the failure line. Once compressive stresses begin to control section capacity they become very important. Minor differences in the shape of the stress-block can have a significant impact on section capacity.

5.3 Veist, Elstner, and Hognestad

The intent of the experimental program conducted by Veist, Elstner, and Hognestad (1956) was to determine the effects of sustained loading on column strength. Tests were thus conducted at both rapid loading rates and very slow loading rates for the purposes of comparing test data to numerically computed data. Only test data for fast loading conditions were used herein. Fast loading as defined in this investigation applies to columns tested to failure in about one hour. The column specimens tested by Veist et al. (1956) were similar to those in Hognestad's 1951 program, however they were cast in a horizontal position. The applied moments at failure were computed using Eq. 15. As noted by Hognestad, a k_3 value of 1.0 predicted the behavior of these horizontally cast columns better than a k_3 value of 0.85 and thus a value of 1.0 was used to compute the analysis results shown in Table 3. All three nonlinear stress strain relationships yielded conservative moment capacities versus the experimental test data.

5.4 Lee and Son

The intent of the Lee and Son (2000) investigation was to verify basic design rules, such as the use of the ACI rectangular stress block, for high strength concrete columns. Thirty-two columns (Figure 11) of various lengths were eccentrically loaded to failure. The columns were

cast horizontally with both low strength and high strength concrete. The additional moment induced by the deflection of the column at midheight upon failure was calculated using Eq. 15. Lee and Son observed that for high strength concrete, the mode of failure was spalling of the concrete cover. It should be noted that the tie spacing was 40 mm for the high strength columns versus 60 mm for the normal strength columns. For analysis purposes, the effects of confinement were not considered. From the results shown in Table 4 several observations can be made:

- Differences in the moment comparison ratios for different stress-strain curves were greater at low load eccentricities, and negligible for high eccentricities.
- For high strength concrete columns, the average moment comparison ratio for Hognestad's stress-strain relationship was 1.04. This is unconservative and in line with previous research noted earlier (e.g. Wee, Chin, and Mansur 1996).
- All stress-strain relationships were less conservative when applied to high strength concrete columns than when applied to normal strength concrete columns.

5.5 Hsu's 1985 Investigation

The primary purpose of the investigation conducted by Hsu (1985) was to examine the deformation and strength of ten L-shaped biaxially loaded columns. The L-shaped columns were 190.5 millimeters by 152.4 millimeters with stem widths of 76.2 millimeters (Figure 12). The columns were set with pinned ends, and subjected to axial loads applied eccentrically in two directions. The column specimens were cast horizontally using normal strength concrete and were reinforced with fourteen #3 bars arranged in such a manner that the plastic centroid and the elastic centroid coincided. In Hsu's computer analysis, strain hardening of steel and the effects of confinement were considered, however they were neglected in the analysis comparison presented this study. The applied moment as amplified by Eq. 15, was already included in the experimental data presented in Hsu (1985) for all specimens except 2a and 3a for which the

amplified moment data was not available. Hence, the moment comparison ratios for these columns are high. By using a k_3 value of 1.0, the predicted analysis results compared reasonably well with the test results, however the standard deviation was high. This may be attributed to the fact that the columns in this investigation were well confined.

5.6 Hsu's 1992 Investigation

The primary purpose of the investigation conducted by Hsu (1992) was to examine the moment curvature relationships of six columns tested in 1974 and 1980. The columns were four inches square (Figure 13), set with pinned ends, and subjected to axial loads applied eccentrically in two directions. The column specimens were cast horizontally using normal strength concrete and were reinforced with nine D5 bars in a symmetric configuration. As in Hsu's original 1985 computer analysis, strain hardening of steel, and the effects of confinement were considered, while they were neglected in this study. The applied moments could not be amplified per Eq. 15 for all columns, thus resulting in high moment comparison ratios. The moment comparison ratios would have been less conservative had strain hardening been taken into account. Using a k_3 value of 1.0, the analysis results corresponding to all three stress-strain curves were reasonably conservative as seen in Table 6.

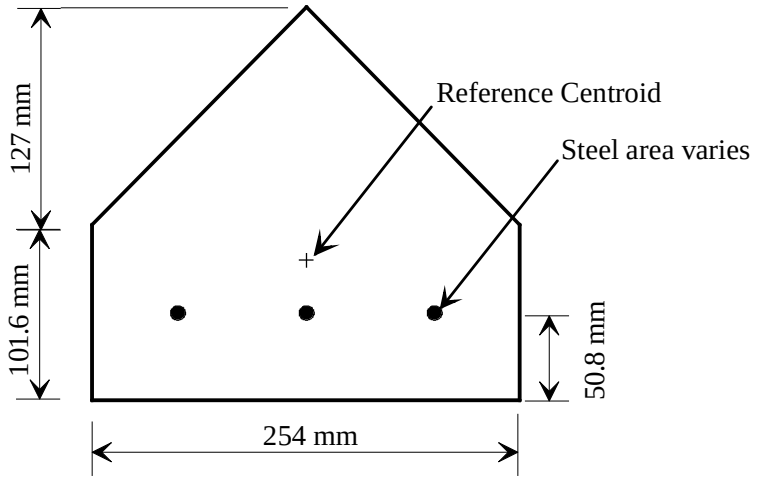

Figure 8. Typical beam specimen Mattock and Kriz (1961)

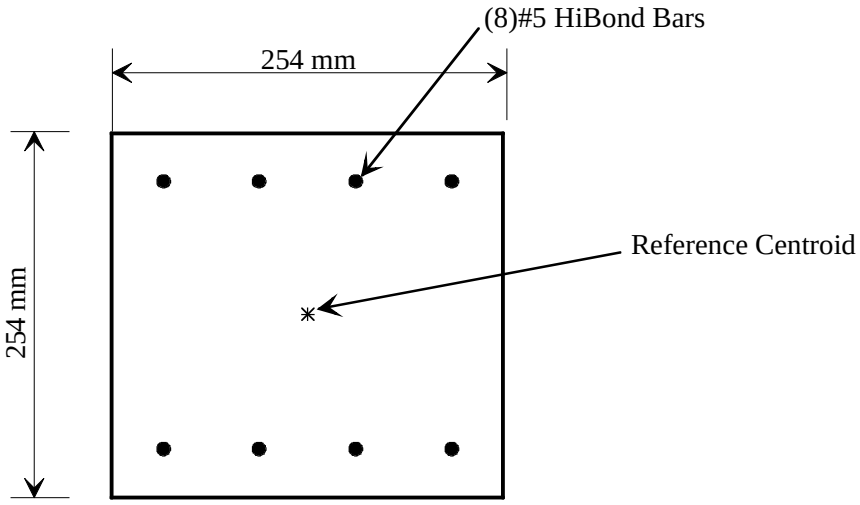

Figure 9. Typical column specimen - Hognestad (1951, Group II)

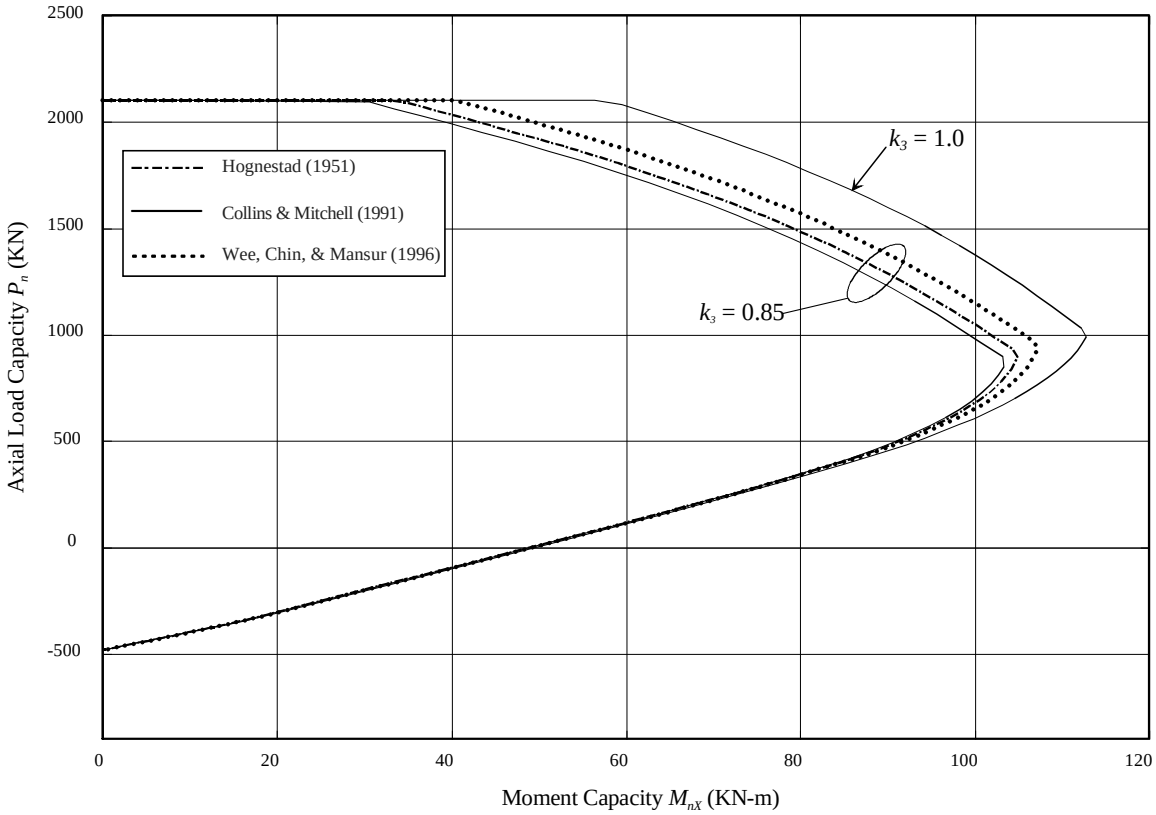

Figure 10. Specimen A-7B - Hognestad (1951, Group II)

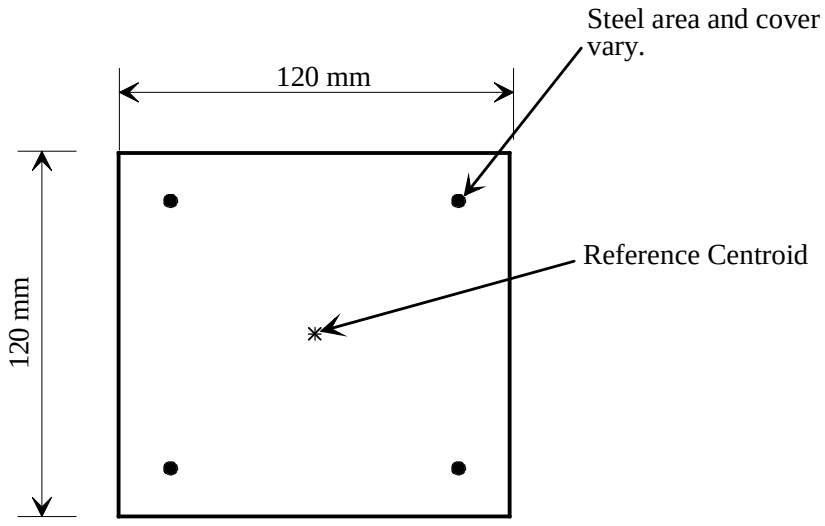

Figure 11. Typical H-series & V-series - Lee and Son (2000)

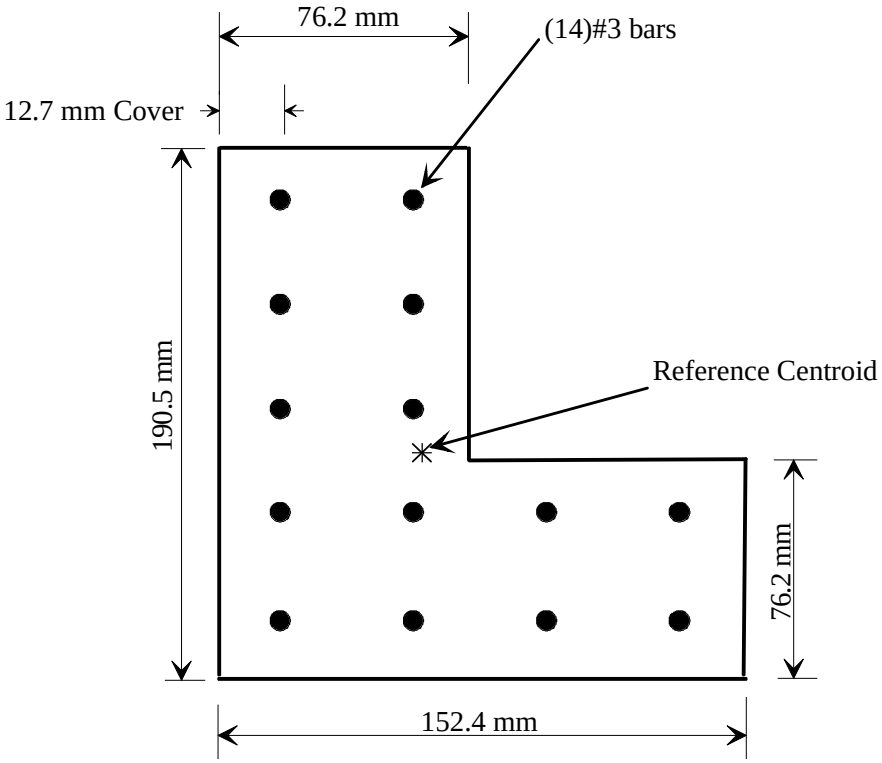

Figure 12. Typical L-shaped column - Hsu (1985)

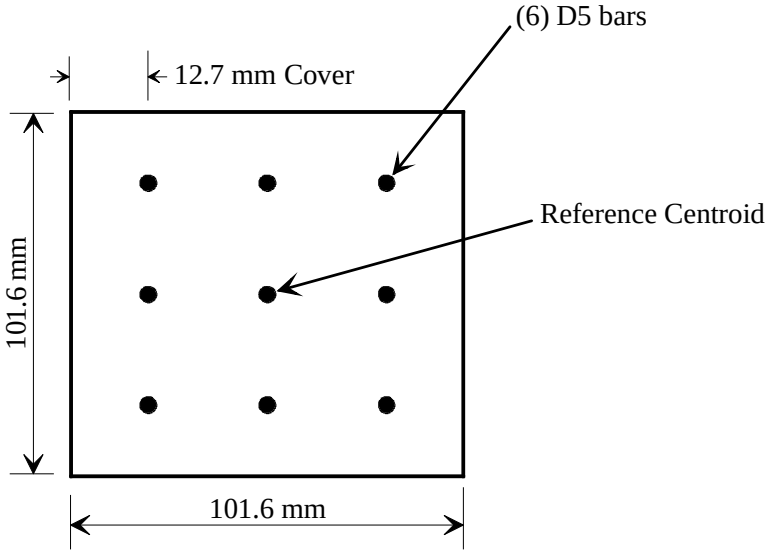

Figure 13. Typical column cross-section - Hsu (1992)

Table 1. Comparison of analysis results versus Mattock & Kriz (1961)

Beam No.	**f'_c** (MPa)	**A_s** (mm^2)	**f_y** (MPa)	**Maximum Concrete Strain (ε_c)**		
				Test	**GSB**	**RSB**
					calculated	assumed
T-1	24.94	568	337.6	0.0037	0.0032	0.003
T-2	23.80	852	337.6	0.0038	0.0040	0.003
T-3	43.34	1161	310.1	0.0035	0.0034	0.003
T-4	11.95	568	341.1	0.0031	0.0040	0.003
T-5	24.12	852	347.9	0.0040	0.0040	0.003
T-6	48.23	1161	310.1	0.0038	0.0032	0.003

	Ultimate Moment (KN-m)					**M(Analysis) / M(Test)**			
	Test	**GSB[1]**	**RSB[2]**	**C&M[3]**	**WCM[4]**	**GSB**	**RSB**	**C&M**	**WCM**
T-1	22.24	22.19	21.98	22.27	22.38	1.00	0.99	1.00	1.01
T-2	27.23	27.48	24.30	25.21	26.22	1.01	0.89	0.93	0.96
T-3	36.94	39.14	36.17	38.75	40.86	1.06	0.98	1.05	1.11
T-4	14.90	15.94	13.15	14.38	14.82	1.07	0.88	0.97	0.99
T-5	29.21	27.69	24.75	25.44	26.45	0.95	0.85	0.87	0.91
T-6	41.63	40.53	36.51	41.05	42.05	0.97	0.88	0.99	1.01
Average Moment Comparison Ratios						**1.01**	**0.91**	**0.97**	**1.00**

1 – General Stress Block
2 – Rectangular Stress Block
3 – Collins and Mitchell (1991)
4 – Wee, Chin, and Mansur (1996)

Table 2. Comparison of Analysis Results Versus Hognestad (1951, Group II)

				At Failure		M (analysis)				M (analysis) / M			
Column ID	**f'_c**	**e**	**y_e**	**P**	**M**	**C&M**	**C&M[1]**	**WCM[2]**	**HOG[3]**	**C&M**	**C&M**	**WCM**	**HOG**
	(MPa)	(mm)	(mm)	(MPa)	(KN-m)	(KN-m)	(KN-m)	(KN-m)	(KN-m)				
k_3 value used in analysis						**1.0**	**0.85**	**0.85**	**0.85**	**1.0**	**0.85**	**0.85**	**0.85**
A-7a	36.10	82.6	4.83	1219	106.54								
A-7b	40.03	63.5	6.60	1264	88.60	104.32	88.45	95.28	91.09	1.18	1.00	1.08	1.03
B-7a	28.11	63.5	6.35	1139	79.57	77.56	64.27	66.46	61.77	0.97	0.81	0.84	0.78
B-7b	27.84	63.5	6.10	1104	76.81	78.55	65.66	67.68	63.04	1.02	0.85	0.88	0.82
C-7a	13.57	63.5	7.11	627	44.31	57.48	49.29	48.62	45.04	1.30	1.11	1.10	1.02
C-7b	10.47	63.5	6.86	564	39.70	49.03	42.04	41.28	38.26	1.24	1.06	1.04	0.96
Average for Columns 7										**1.14**	**0.97**	**0.99**	**0.92**
A-8a	38.03	127.0	8.64	721	97.78	103.97	98.01	100.97	99.60	1.06	1.00	1.03	1.02
A-8b	40.03	127.0	10.16	676	92.78	103.49	99.20	101.00	99.87	1.12	1.07	1.09	1.08
B-8a	32.38	127.0	8.89	694	94.33	98.36	93.27	94.66	93.05	1.04	0.99	1.00	0.99
B-8b	29.35	127.0	8.13	650	87.79	94.31	89.52	90.39	88.79	1.07	1.02	1.03	1.01
C-8a	12.40	127.0	8.13	441	59.53	64.90	57.86	57.52	53.87	1.09	0.97	0.97	0.90
C-8b	12.40	127.0	9.91	441	60.31	64.90	57.86	57.52	53.87	1.08	0.96	0.95	0.89
Average for Columns 8										**1.08**	**1.00**	**1.01**	**0.98**
A-9a	35.14	190.5	9.40	396	79.17	84.47	82.98	83.47	83.07	1.07	1.05	1.05	1.05
A-9b	35.62	190.5	9.91	406	81.33	85.33	83.77	84.33	83.88	1.05	1.03	1.04	1.03
B-9a	32.38	190.5	8.89	418	83.40	85.34	83.40	83.92	83.33	1.02	1.00	1.01	1.00
B-9b	30.11	190.5	8.13	398	79.11	83.21	81.37	81.75	81.15	1.05	1.03	1.03	1.03
C-9a	12.95	190.5	9.65	325	65.02	68.81	65.98	65.45	62.49	1.06	1.01	1.01	0.96
C-9b	11.92	190.5	8.89	291	58.12	66.78	64.29	63.80	61.52	1.15	1.11	1.10	1.06
Average for Columns 9										**1.07**	**1.04**	**1.04**	**1.02**
A-10a	35.14	317.5	7.11	205	66.59	68.27	67.50	67.69	67.53	1.03	1.01	1.02	1.01
A-10b	35.62	317.5	6.35	196	63.41	67.50	66.73	66.93	66.77	1.06	1.05	1.06	1.05
B-10a	29.35	317.5	7.11	194	62.84	66.40	65.73	65.79	65.67	1.06	1.05	1.05	1.05
B-10b	30.11	317.5	7.37	196	63.61	66.71	66.03	66.11	65.97	1.05	1.04	1.04	1.04
C-10a	15.85	317.5	8.89	198	64.63	64.44	63.77	63.63	63.30	1.00	0.99	0.98	0.98
C-10b	12.20	82.6	9.65	200	65.51	63.28	62.10	61.86	61.40	0.97	0.95	0.94	0.94
Average for Columns 10										**1.03**	**1.01**	**1.01**	**1.01**
Total Average Moment Comparison Ratios										**1.08**	**1.01**	**1.01**	**0.99**

1 – Collins and Mitchell (1991)

2 – Wee, Chin, and Mansur (1996)

3 – Hognestad (1951)

Table 3. Comparison of analysis results versus (Hognestad 1956)

				At failure		P(calc)
Column	**f'_c**	**e**	**y_e**	**P**	**M**	**GSB**
	(MPa)	(mm)	(mm)	(KN)	(KN-m)	(KN)
20B1a	15.78	92.2	4.85	120	11.66	108
20B1b	14.61	96.8	4.80	98	9.99	101
35B1a	29.21	63.5	5.23	219	15.08	200
35B1b	32.80	57.2	4.57	214	13.18	235
50B1a	37.00	57.2	5.89	263	16.55	249
50B1b	30.04	63.5	4.04	223	15.03	202
20C1a	20.53	31.8	3.81	256	9.11	249
20C1b	10.75	44.5	4.60	151	7.42	148
20C1c	2440	31.8	3.66	223	7.88	221
35C1a	16.81	31.8	3.89	312	11.10	299
35C1b	29.49	44.5	5.11	240	11.91	260

	M(analysis)			P/P(calc)	M(analysis) / M		
	C&M[1]	**WCM[2]**	**HOG[3]**	**GSB[4]**	**C&M**	**WCM**	**HOG**
	(KN-m)	(KN-m)	(KN-m)				
20B1a	11.30	10.34	9.78	0.90	0.88	0.89	0.84
20B1b	10.25	10.20	9.92	1.02	1.03	1.02	0.99
35B1a	12.53	13.11	12.57	0.91	0.83	0.87	0.83
35B1b	13.72	14.25	13.94	1.10	1.04	1.08	1.06
50B1a	14.00	14.93	14.49	0.95	0.85	0.90	0.88
50B1b	12.71	13.34	12.81	0.91	0.85	0.89	0.85
20C1a	8.49	8.56	7.99	0.97	0.93	0.94	0.88
20C1b	7.05	6.98	6.54	0.98	0.95	0.94	0.88
20C1c	7.78	7.77	7.23	0.99	0.99	0.99	0.92
35C1a	9.57	10.06	9.47	0.96	0.86	0.91	0.85
35C1b	12.16	12.76	12.21	1.08	1.02	1.07	1.03
Average Moment Comparison Ratios				**0.98**	**0.93**	**0.95**	**0.91**

1 – Collins and Mitchell (1991)

2 – Wee, Chin, and Mansur (1996)

3 – Hognestad (1951)

4 – General Stress Block (Hognestad 1951)

Table 4. Comparison of analysis results versus Lee & Son (2000)

Column		At Failure			M (analysis)				M(analysis) / M			
	f'_c	y_e	P	M	RSB[1]	C&M[2]	WCM[3]	HOG[4]	RSB	C&M	WCM	HOG
	(Mpa)	(mm)	(KN)	(KN-m)	P(analysis)	(KN-m)	(KN-m)	(KN-m)	P(analysis)			
LS-1	41.76	21.2	736.30	15.62	667.27	11.61	13.70	12.74	0.91	0.74	0.88	0.82
LS-2	41.76	47.3	371.15	17.57	344.14	16.60	17.20	16.92	0.93	0.94	0.98	0.96
LS-3	41.76	69.3	173.07	11.99	172.07	11.82	11.96	11.86	0.99	0.99	1.00	0.99
LM-1	41.76	27.0	653.26	17.65	554.22	13.77	15.54	14.76	0.85	0.78	0.88	0.84
LM-2	41.76	57.5	360.15	20.72	248.10	16.49	17.06	16.78	0.69	0.80	0.82	0.81
LM-3	41.76	76.1	146.06	11.11	149.06	10.84	10.94	10.90	1.02	0.98	0.98	0.98
LL-1	34.87	37.5	413.17	15.51	378.15	14.22	15.23	14.68	0.92	0.92	0.98	0.95
LL-2	34.87	66.8	172.07	11.49	177.07	11.45	11.55	11.36	1.03	1.00	1.01	0.99
LL-3	34.87	81.1	108.04	8.76	116.05	9.03	9.12	9.03	1.07	1.03	1.04	1.03
HS-1	70.33	25.9	529.21	13.72	546.22	14.40	15.68	16.21	1.03	1.05	1.14	1.18
HS-2	70.33	47.8	333.13	15.94	310.13	15.89	16.32	16.42	0.93	1.00	1.02	1.03
HS-3	70.33	68.6	187.08	12.82	173.07	12.67	12.78	12.81	0.93	0.99	1.00	1.00
HM-1	70.33	28.1	508.21	14.29	526.21	14.76	15.93	16.49	1.04	1.03	1.11	1.15
HM-2	70.33	55.8	307.12	17.15	263.11	15.54	15.86	16.00	0.86	0.91	0.92	0.93
HM-3	70.33	75.2	156.06	11.73	149.06	11.61	11.61	11.55	0.96	0.99	0.99	0.98
HL-1	70.33	39.7	523.21	20.79	395.16	14.51	15.75	16.32	0.76	0.70	0.76	0.78
HL-2	70.33	63.4	205.08	13.01	202.08	13.24	13.38	13.38	0.99	1.02	1.03	1.03
HL-3	70.33	80.0	118.05	9.44	129.05	9.98	10.05	10.05	1.09	1.06	1.07	1.07
HS-1A	70.33	26.3	669.27	17.62	596.24	16.23	17.74	18.45	0.89	0.92	1.01	1.05
HS-3A	70.33	68.0	340.14	23.11	312.13	22.32	23.40	23.50	0.92	0.97	1.01	1.02
HM-1A	70.33	26.5	631.26	16.74	616.25	17.08	18.59	19.25	0.98	1.02	1.11	1.15
HM-3A	70.33	75.5	273.11	20.61	280.11	21.99	22.37	22.41	1.03	1.07	1.09	1.09
HL-1A	70.33	43.5	488.20	21.25	428.17	19.82	21.14	22.08	0.88	0.93	0.99	1.04
HL-3A	70.33	88.3	216.09	19.07	222.09	20.81	20.86	20.86	1.03	1.09	1.09	1.09
VS-1	93.11	27.6	655.27	18.10	694.28	18.89	19.53	21.35	1.06	1.04	1.08	1.18
VS-2	93.11	47.7	416.17	19.87	419.17	20.07	20.35	20.96	1.01	1.01	1.02	1.06
VM-1	93.11	28.2	639.26	18.04	666.27	19.13	19.66	21.52	1.04	1.06	1.09	1.19
VM-2	93.11	58.5	324.13	18.98	320.13	18.58	18.58	18.80	0.99	0.98	0.98	0.99
VS-1A	93.11	27.3	831.34	22.71	776.31	18.95	19.66	22.30	0.93	0.83	0.87	0.98
VS-2A	93.11	47.4	531.21	25.20	528.21	23.91	24.62	27.31	0.99	0.95	0.98	1.08
VM-1A	93.11	30.5	796.32	24.31	729.29	19.66	20.38	22.95	0.92	0.81	0.84	0.94
VM-2A	93.11	57.0	475.19	27.11	446.18	24.52	25.39	27.31	0.94	0.90	0.94	1.01
Average of Total									**0.96**	**0.95**	**0.99**	**1.01**
Average of normal strength columns (L-series)									0.93	0.91	0.95	0.93
Average of high strength columns (H-series and V-series)									0.96	0.97	1.01	1.04
Average of high strength columns (low reinforcement ratio)									0.97	0.99	1.02	1.04
Average of high strength columns (high reinforcement ratio)									0.95	0.95	0.99	1.05
Average of low strength columns with low eccentricity.										0.81	0.91	0.87
Average of low strength columns with medium eccentricity										0.91	0.94	0.92
Average of low strength columns with high eccentricity										1.00	1.01	1.00
Average of high strength columns with low eccentricity.										0.93	1.01	1.04
Average of high strength columns with medium eccentricity.										0.97	0.99	1.00
Average of high strength columns with high eccentricity.										1.01	1.02	1.02

1 – Rectangular Stress Block
2 – Collins and Mitchell (1991)
3 – Wee, Chin, and Mansur (1996)
4 – Hognestad (1951)

Table 5. Comparison of analysis results versus Hsu (1985)

					At Failure				
Column	**f'_c**	**f_y**	**e_x**	**e_y**	**P**	**M_X**	**M_Y**	**M_R**	**α**
	(MPa)	(MPa)	(mm)	(mm)	(KN)	(KN-m)	(KN-m)	(KN-m)	
2a[1]	25.88	356.90	16.33	16.33	495.73	8.10	8.10	11.45	45.0
3a[1]	25.67	356.90	35.38	-9.07	284.80	-2.58	10.08	10.40	-14.4
4b	28.94	461.63	38.86	127.00	169.99	23.17	9.02	24.86	68.8
5b	28.94	461.63	42.67	139.70	156.20	24.41	9.58	26.23	68.6
6b	27.56	399.62	42.67	165.10	119.26	21.27	6.91	22.37	72.1

	Collins & Mitchell			**Wee, Chin, and Mansur**			**Hognestad**			**M_{nR}(analysis) / M_R**		
	M_{nX}	**M_{nY}**	**M_{nR}**	**M_{nX}**	**M_{nY}**	**M_{nR}**	**M_{nX}**	**M_{nY}**	**M_{nR}**	**C&M[2]**	**WCM[3]**	**HOG[4]**
	(KN-m)	(KN-m)	(KN-m)	(KN-m)	(KN-m)	(KN-m)	(KN-m)	(KN-m)	(KN-m)			
2a	8.28	8.28	11.71	8.45	8.45	11.96	8.16	8.16	11.54	1.02	1.04	1.01
3a	-3.89	13.86	14.39	-4.09	14.34	14.92	-3.62	13.70	14.17	1.38	1.43	1.36
4b	16.27	6.28	17.44	16.76	6.59	18.01	16.27	6.36	17.47	0.70	0.72	0.70
5b	16.27	6.44	17.50	16.39	6.67	17.70	16.15	6.44	17.38	0.67	0.67	0.66
6b	15.88	5.17	16.70	16.15	5.24	16.98	15.81	5.20	16.65	0.75	0.76	0.74
Average Moment Comparison Ratios										**0.90**	**0.93**	**0.90**

1 – M_X, M_Y, and M_R were not amplified per Eq. (15)

2 – Collins and Mitchell (1991)

3 – Wee, Chin, and Mansur (1996)

4 – Hognestad (1951)

Table 6. Comparison of analysis results Vs. (Hsu 1992)

							At Failure					
Column	**f'_c**	**f_y**	**e_x**	**e_y**	**δ_{ex}**	**δ_{ey}**	**P**	**M_X**	**M_Y**	**M_R**	**α**	
	(MPa)	(MPa)	(mm)	(mm)	(mm)	(mm)	(KN)	(KN-m)	(KN-m)	(KN-m)		
U-1	26.91	502.97	63.5	88.9	0.00	0.00	42.72	3.80	2.71	4.67	26.91	
U-2	26.22	502.97	76.2	88.9	0.00	0.00	38.72	3.44	2.95	4.53	26.22	
U-3	26.83	502.97	88.9	88.9	8.05	8.05	35.60	3.45	3.45	4.88	26.83	
U-4	26.39	502.97	50.8	50.8	8.41	8.41	63.64	3.77	3.77	5.33	26.39	
U-5	25.60	502.97	12.7	101.6	1.80	13.92	48.06	5.55	0.70	5.60	25.60	
U-6	26.84	502.97	12.7	177.8	1.30	16.15	27.77	5.39	0.39	5.40	26.84	
	Collins & Mitchell			**Wee, Chin, & Mansur**			**Hognestad**			**M_{nR}(analysis) / M_R**		
	M_{nX}	**M_{nY}**	**M_{nR}**	**M_{nX}**	**M_{nY}**	**M_{nR}**	**M_{nX}**	**M_{nY}**	**M_{nR}**	**C&M**	**WCM**	**HOG**
	(KN-m)	(KN-m)	(KN-m)	(KN-m)	(KN-m)	(KN-m)	(KN-m)	(KN-m)	(KN-m)			
U-1	3.44	2.49	4.25	3.53	2.55	4.36	3.44	2.47	4.24	0.91	0.93	0.91
U-2	3.13	2.71	4.14	3.19	2.77	4.23	3.10	2.71	4.12	0.91	0.93	0.91
U-3	2.93	2.93	4.15	2.99	2.99	4.23	2.91	2.91	4.11	0.85	0.87	0.84
U-4	2.96	2.96	4.19	3.05	3.05	4.31	2.93	2.93	4.15	0.79	0.81	0.78
U-5	4.87	0.63	4.91	4.94	0.65	4.98	4.83	0.65	4.87	0.88	0.89	0.87
U-6	4.87	0.37	4.88	4.89	0.37	4.91	4.85	0.39	4.86	0.90	0.91	0.90
Average Moment Comparison Ratios										**0.87**	**0.89**	**0.87**

CHAPTER 6
CONCLUSIONS AND COMMENTARY

The numerical procedure described in this thesis provides researchers and designers with a powerful new tool for concrete column analysis by which sections of arbitrary shape and reinforcement pattern can be analyzed and studied in an efficient manner. This is achieved by extracting two-dimensional interaction diagrams from a mesh of computed failure points on the three-dimensional failure surface. The accuracy of the two-dimensional interaction diagrams can be increased to any desired level by increasing the number of neutral axis orientations and positions used to generate the failure points.

For each position and orientation of the neutral axis, the numerical procedure rotates the cross-section and discretizes it in such a manner that the forces in the underlying materials can be determined, and thus also the failure point. The numerical procedure can accommodate any cross-sectional shape since it does not rely on curve fitting solutions to describe the three-dimensional failure surface. Designers using the interaction diagrams generated by the numerical procedure must take care to adjust the location of the applied axial load determined in frame analysis software such that the applied axial load occurs at the location of the reference centroid on the cross-section. This is because the moment capacity of the cross-section is determined by summing the internal forces developed in the constituent materials about the reference centroid.

The effectiveness of the proposed model has been demonstrated and validated by comparing analysis results to experimental results contained in the literature. The underlying assumptions made for material behavior in the model can be modified to suit the needs designers and researchers, however before doing so it is important to understand the ramifications of making such changes.

Concrete stress-strain curves are just one example of how the assumptions used in the proposed model may be modified for special situations. In this study, non-linear concrete stress-strain curves were used in place of the traditional rectangular stress block. The ease with which various stress-strain functions can be written and inserted into the program provides researchers with a powerful tool for using nonlinear stress-strain functions derived specifically for experimental investigations.

Designers must be careful to use a concrete stress-strain relationship that is applicable. For example, it has been shown in the literature and in this thesis that Hognestad's stress-strain model will yield un-conservative moment capacities if applied to columns made of high strength concrete. In the comparison study presented in this thesis the concrete stress-strain relationship presented by Wee, Chin, and Mansur (1996) produced the most accurate analysis results. The stress-strain curve by Collins and Mitchell (1991) was slightly more conservative than Wee, Chin and Mansur (1996).

It has also been shown that the shape of the stress-strain curve for concrete is less important for sections in pure flexure than for sections carrying substantial axial load. While it has been shown in the literature that the rectangular stress block can be applied conservatively to beams with nonrectangular compressive zones, nonlinear stress-strain curves yield more accurate results. Hence designers may opt to use nonlinear stress-strain curves for beams and columns to economize design.

More research is needed for an accurate determination of k_3. As discussed in this thesis, published research shows conflicting values and relationships for k_3. It is the belief of this author that k_3 as defined in this thesis is a function of casting position, concrete strength type, slump, water-cement ratio, admixtures and curing rate. For design, specimens cast vertically

should have a lower value of k_3 than specimens cast horizontally due to weaker concrete at the top of the specimen. Some research has shown the value of k_3 to be higher for high strength concrete than for low strength concrete. Experimental testing is needed on a much larger scale if reliable conclusions are to be drawn and guidelines established via codification.

In the mean time, for horizontally cast beams subjected to flexural bending only, a k_3 value of unity has been shown to be appropriate for all concrete strength types. Also a value of unity can be used for tilt-up wall panels since these members are typically only six to twelve inches in thickness and are also cast horizontally. For normal strength concrete in columns cast vertically and deep beams cast horizontally, a value of 0.85 is reasonable based on the comparison of analysis data to test results from Hognestad's 1951 experimental investigation. For high strength concrete columns cast vertically and deep beams, an appropriate value for k_3 is hard to discern from the available literature. Based on the literature a value of 0.85 appears to be reasonable choice until more definitive information is available. In addition, engineers must consider information specific to each project and apply their engineering judgment accordingly.

APPENDIX A
PROGRAMMING FUNCTIONS

The following functions are self-contained modules that can be inserted into the program described herein to represent concrete stress-strain relationships. For the functions listed in Appendix A, f_c is the peak compressive stress of the test cylinders as specified by the designer.

$$\text{Location}_{peak}(f'_c) := \left| \begin{array}{l} \varepsilon_o \leftarrow 0.002 \\ \text{return } \varepsilon_o \end{array} \right.$$

$$f_{cs}(f'_c, \varepsilon) := \left| \begin{array}{l} f_c \leftarrow k_3 \cdot f'_c \\ \varepsilon_o \leftarrow 0.002 \\ f_{cs\_actual} \leftarrow f_c \cdot \left[(2) \cdot \left(\frac{\varepsilon}{\varepsilon_o} \right) - \left(\frac{\varepsilon}{\varepsilon_o} \right)^2 \right] \\ \text{return } f_{cs\_actual} \end{array} \right.$$

Figure 14. Hognestad's stress-strain function

$$f_{cs}(f'_c, \varepsilon) := \left| \begin{array}{l} f_c \leftarrow k_3 \cdot f'_c \\ n \leftarrow \frac{1}{2.5} \cdot f_c + 0.8 \\ E_c \leftarrow 1265\sqrt{f_c} + 1000 \\ \varepsilon_o \leftarrow \frac{f_c}{E_c} \cdot \left(\frac{n}{n-1} \right) \\ k \leftarrow \max\left(1.0, \frac{f_c}{9} + 0.67 \right) \\ fcs_{ascending} \leftarrow \frac{f_c \cdot n \cdot \left(\frac{\varepsilon}{\varepsilon_o} \right)}{n - 1 + \left(\frac{\varepsilon}{\varepsilon_o} \right)^n} \\ fcs_{descending} \leftarrow \frac{f_c \cdot n \cdot \left(\frac{\varepsilon}{\varepsilon_o} \right)}{n - 1 + \left(\frac{\varepsilon}{\varepsilon_o} \right)^{n \cdot k}} \\ fcs\_actual \leftarrow \left| \begin{array}{ll} fcs_{ascending} & \text{if } \varepsilon < \varepsilon_o \\ fcs_{descending} & \text{if } \varepsilon \geq \varepsilon_o \end{array} \right. \\ \text{return } fcs\_actual \end{array} \right.$$

$$Location_{peak}(f'_c) := \left| \begin{array}{l} f_c \leftarrow k_3 \cdot f'_c \\ n \leftarrow \frac{1}{2.5} \cdot f_c + 0.8 \\ E_c \leftarrow 1265\sqrt{f_c} + 1000 \\ \varepsilon_o \leftarrow \frac{f_c}{E_c} \cdot \left(\frac{n}{n-1} \right) \\ \text{return } \varepsilon_o \end{array} \right.$$

f_c is the peak compressive stress of the test cylinders (ksi) as specified by the designer.

Figure 15. Collins & Mitchell's stress-strain function

$$f_{cs}(f'_c, \varepsilon) :=$$

$f'_c \leftarrow k_3 \cdot (f'_c \cdot 6.89)$

$E_{it} \leftarrow (10200) \cdot f'_c^{\frac{1}{3}}$

$\varepsilon_o \leftarrow (.00078) \cdot f'_c^{0.25}$

$\beta \leftarrow \dfrac{1}{1 - \left(\dfrac{f'_c}{\varepsilon_o \cdot E_{it}}\right)}$

$k_1 \leftarrow \begin{cases} \left(\dfrac{50}{f'_c}\right)^{3.0} & \text{if } f'_c > 50 \\ 1.0 & \text{if } f'_c \le 50 \end{cases}$

$k_2 \leftarrow \begin{cases} \left(\dfrac{50}{f'_c}\right)^{1.3} & \text{if } f'_c > 50 \\ 1.0 & \text{if } f'_c \le 50 \end{cases}$

$fcs_{ascending} \leftarrow f'_c \cdot \left[\dfrac{\beta \cdot \left(\dfrac{\varepsilon}{\varepsilon_o}\right)}{\beta - 1 + \left(\dfrac{\varepsilon}{\varepsilon_o}\right)^{\beta}}\right]$

$fcs_{descending} \leftarrow f'_c \cdot \left[\dfrac{k_1 \cdot \beta \cdot \left(\dfrac{\varepsilon}{\varepsilon_o}\right)}{k_1 \cdot \beta - 1 + \left(\dfrac{\varepsilon}{\varepsilon_o}\right)^{k_2 \cdot \beta}}\right]$

$fcs \leftarrow \begin{cases} fcs_{ascending} & \text{if } \varepsilon < \varepsilon_o \\ fcs_{descending} & \text{if } \varepsilon \ge \varepsilon_o \end{cases}$

$fcs\_actual \leftarrow \dfrac{fcs}{6.89}$

return fcs_actual

$$Location_{peak}(f'_c) :=$$

$f'_c \leftarrow k_3 \cdot (f'_c \cdot 6.89)$

$\varepsilon_o \leftarrow (.00078) \cdot f'_c^{0.25}$

return ε_o

f_c is the peak compressive stress of the test cylinders (ksi) as specified by the designer.

Figure 16. Wee, Chin, & Mansur's stress-strain function

REFERENCES

Ansley, M. (2001), "Program for computing load-moment interaction diagrams for columns under biaxial flexure," Available for download from the Florida DOT Structures Design Office website (www.dot.state.fl.us/structures), Posted 2001.

Attard, M. M., and Stewart, M. G. (1998), *A Two Parameter Stress Block for High-Strength Concrete*, ACI Structural Journal, Vol. 95, No. 3, May-June 1998, pp. 305-317.

Bartlett, F. M., and MacGregor, J. G. (1996), *Statistical Analysis of the Compressive Strength of Concrete in Structures*, ACI Materials Journal, Vol. 93, No. 2, 1996, pp. 158-168.

Collins, M. P., and Mitchell, D. (1991), *Prestressed Concrete Structures*, Prentice-Hall, Englewood Cliffs, N. J.

Hognestad, E., Hanson, N. W., McHenry, D. (1955), *Concrete Stress Distribution in Ultimate Strength Design*, ACI Journal, Vol. 27, No. 4, Dec 1955, pp. 455-477.

Hognestad E. (1951), *A Study of Combined Bending and Axial Load in Reinforced Concrete Members*, University of Illinois Engineering Experiment Station, Bulletin Series No. 399, 1951.

Hsu, C.-T T. (1985), *Biaxially Loaded L-Shaped Reinforced Concrete Columns*, Journal of Structural Engineering, ASCE, Vol. 111, No. 12, December 1985, pp. 2576-2595.

Ibrahim, H. H. H., and MacGregor, J. G. (1997), *Modification of the ACI Rectangular Stress Block for High-Strength Concrete*, ACI Structural Journal, Vol. 94, No. 1, Jan-Feb 1997, pp. 40-48.

Kennedy, H. L. (1951), *High Strength Concrete*, Proceedings of the First U. S. Conference on Prestressed Concrete, Massachusetts Institute of Technology, Cambridge, Aug 1941, pp.126-135.

Lee, J-H., and Son, H-S (2000), *Failure and Strength of High-Strength Concrete Columns Subjected to Eccentric Loads*, ACI Structural Journal, Vol. 97, No. 1, Jan-Feb 2000, pp. 75-85.

Mansur, M. A., Chin, M. S., Wee, T. H. (1997), *Flexural Behavior of High-Strength Concrete Beams*, ACI Structural Journal, Vol. 94, No. 6, Nov-Dec 1997, pp. 663-674.

Mattock, A. H., and Kriz, L. B. (1961), *Ultimate Strength of Nonrectangular Structural Concrete Members*, ACI Journal, Vol. 32, No. 7, Jan 1961, pp. 737-766.

Rodriguez-Gutierrez, J. A., and Aristizabal-Ochoa, J. D. (1999), *Biaxial Interaction Diagrams for Short RC Columns of Any Cross Section*, Journal of Structural Engineering, ASCE, Vol. 125, No. 6, 1999, pp. 671-683.

Slater, W. A. and Lyse, I. (1931), *First Progress Report on Column Tests at Lehigh University*, ACI Journal, Vol. 27, Feb 1931, pp. 677-730

Viest, I. M., Elstner, R. C., and Hognestad, E. (1956), *Sustained Load Strength of Eccentrically Loaded Short Reinforced Concrete Columns*, ACI Journal, Vol. 27, No. 7, March 1956, pp. 727-755.

Wang, G. G., and Hsu, Cheng-Tzu Thomas (1992), *Complete Biaxial Load-Deformation Behavior of RC Columns*, Journal of Structural Engineering, ASCE, Vol. 118, No. 9, September 1992, pp. 2590-2609.

Wang, P. T., Shah, S. P., and Naaman, A. E. (1978), *Stress-Strain Curves of Normal and Lightweight Concrete in Compression*, ACI Journal, Vol. 75, No. 11, 1978, pp. 603-611.

Wee, T. H., Chin, M. S., and Mansur, M. A. (1996), *Stress-Strain Relationship of High-Strength Concrete in Compression*, Journal of Materials in Civil Engineering, ASCE, Vol. 8, No. 2, May 1996, pp. 70-76.

Biaxial Concrete Column Analysis and Nonlinear Stress-Strain Curves - Quiz

Updated: 10/25/2018

1. A three dimensional interaction diagram is a visual presentation of all the following forces except for _____.

    a) axial compression
    b) bending moment about the X-axis
    c) torsion about the Z-axis
    d) bending moment about the Y-axis

2. A constant-load biaxial moment interaction diagram can be extracted from the three dimensional interaction diagram by taking a slice through the failure surface at a constant _____.

    a) axial load
    b) torsion load
    c) moment about the X-axis
    d) moment at a specified angle

3. What is the oldest stress-strain curve studied in this study?

    a) Wee, Chin, and Mansur
    b) The Rectangular Stress Block
    c) Hognestad's parabola
    d) Collins and Mitchell

4. €$_o$ represents the strain value on a stress-strain curve that coincides with the maximum stress. What are two other common variables in the stress-strain curves studied in this course that effect the shape of the stress-strain curve?

    a) x
    b) n and various k factors
    c) fy
    d) f'm

5. The numerical method discussed in this course and utilized by FDOT's biaxial column analysis program forms the three dimensional interaction diagram by plotting numerous P-M failure lines. Each P-M load contour or failure line corresponds to a different _____ of orientation for the neutral axis. Each failure point on the P-M failure line represents a different position of the neutral axis in relation to the reference point.

    a) angle
    b) height
    c) position
    d) length

6. As the neutral axis is moved across the cross-section for a fixed θ, the axial load capacity will decrease and the section moment capacities Mx and My will increase. For each location of the neutral axis, the axial load capacity and local moments are computed with respect to the corresponding strain distribution.

    a) True
    b) False

7. Concrete forces are determined by the program by multiplying multiple segment areas by the known strain at each segment using which integration technique

    a) Calculus
    b) Simpson's rule
    c) Curve fitting
    d) none of the above

8. The accuracy of the three dimensional failure surface and the accuracy of the extracted constant-load interaction diagrams are improved by increasing the number of _____ orientations analysed.

    a) compression zone
    b) rebar
    c) stress-strain curve
    d) neutral axis

9. The numerical procedure utilized in this study and employed by FDOT's biaxial load program determine moments by summing forces about the _____.

    a) bottom of the section
    b) reference centroid
    c) top of the section
    d) neutral axis

10. Utilizing non-linear stress-strain curves instead of the lower bound rectangular stress block result in _____ capacities for the given concrete sections.

a) higher
b) lower
c) the same
d) variable

11. When using non-linear stress strain curves in concrete analysis it is important to accurately represent the in situ strength of the concrete. The strength of the in situ concrete can be different then what the concrete reference test cylinder breaks predict. What factor is used to adjust for these differences?

a) beta
b) k_3
c) fc
d) all of the above

12. What is the most significant factor contributing to the difference between in situ concrete strength and the strength predicted by concrete test cylinders?

a) Formwork types
b) heat of hydration
c) casting position and depth of pour
d) loading rate

13. The rectangular stress block cannot be used with non-rectangular sections.

a) True
b) False

14. The shape of the stress-strain block is more important for concrete analysis of column than beams because a larger percentage of their cross section is in _____.

a) compression
b) tension
c) torsion
d) bending

15. When analysing members cast vertically using a nonlinear stress strain block an appropriate value of k3 is _____.

a) 0.65
b) 0.75
c) 0.85
d) 1.0

16. Lee and Son's 2000 investigation showed that all of the nonlinear stress-strain curves were less conservative when comparing test results using high strength concrete. _____ stress-strain curve was unconservative and should not be used when analysing high strength concrete sections.

a) Hognestad's curve (1951)
b) Collins and Mitchell's curve (1991)
c) Wee, Chin, and Mansur's curve (1996)
d) None of the above

17. When analysing columns that are primarily in compression with little eccentric loading the accuracy of the stress-strain curve and the proper selection of the k3 value is more important than when analysing beams. If casting position is ignored and a value of k3 of unity is used, the analysis results may be unconservative.

a) True
b) False

18. Which nonlinear stress-strain curve yielded the most accurate results in this study.

a) Collins and Mitchell (1991)
b) Hognestad (1951)
c) Wee, Chin, and Mansur (1996)
d) The Rectangular Stress Block

19. Nonlinear stress-strain curves have been shown to be more accurate for
a) columns
b) beams
c) columns and beams
d) none of the above because they were less accurate

20. What is a reasonable value of k3 when casting tilt-up wall panels
    a) 0.65
    b) 0.75
    c) 0.85
    d) 1.0